nature communications

Article

https://doi.org/10.1038/s41467-025-66107-x

Differential modulation of feedforward inhibition reflects topographic organization in the olfactory system

Received: 29 July 2024

Accepted: 30 October 2025

Published online: 16 December 2025

Check for updates

Julius Jonaitis[1,2,3], Mohd F. E. B. Mazri[1,3], John W. Hageter[1], Oliver Cook[1], Tyler R. Sizemore[1], Marryn M. Bennett[1], Jacob D. Ralston[1], Farzaan Salman[1], Emma J. Fletcher[1], Danielle E. Matheny[1], Johnston Renton[1], Keshav L. Ramachandra, Eric J. Horstick[1] & Andrew M. Dacks[1,2]

The nervous system flexibly processes information under different conditions. To do this, neural networks frequently rely on uniform expression of modulatory receptors by distinct classes of neurons to fine tune the computations supported by each neuronal class. Here, we explore an alternate organization in which one population of neurons in the olfactory system of *Drosophila* expresses all of the receptors for the modulator serotonin. We find extensive, heterogeneous receptor co-expression by ventral projection neurons (v-PNs), with many receptor combinations present. Despite overlap in glomerular innervation of v-PNs expressing each serotonin receptor, their axon terminals innervate largely distinct zones within a higher order olfactory region. Serotonin differentially modulates odor-evoked responses of v-PNs with distinct receptor expression and these v-PNs synapse upon separate sets of third order olfactory neurons. This functional organization implies that serotonin differentially modulates the responses of v-PNs that participate in divergent, downstream olfactory circuits.

Within a sensory network, distinct neuronal classes each serve different roles to influence the fidelity with which the nervous system can encode information. For instance, inhibitory local interneurons (LNs) in the mammalian olfactory bulb and insect antennal lobe (AL; first olfactory neuropil of *Drosophila*) provide presynaptic inhibition of sensory afferents within the context of high stimulus intensity to avoid saturation of the olfactory system[1–7]. In this manner, one neuronal class impacts the encoding of a stimulus parameter within the context of ongoing sensory processing. Neuromodulation provides an elegant means by which to adjust the impact of individual network components, and the computations that they support, based on the ongoing behavioral state of the individual animal[8–10]. Neuromodulators usually activate several receptor proteins, which allows a single signaling molecule to differentially affect cellular components that support distinct aspects of sensory coding. Often, a given neuronal class will express a consistent set of modulatory receptors, such that the entire population is affected in a similar manner and the neuronal computation that they exert can be uniformly altered[11]. For instance, a subset of GABAergic LNs in the antennal lobe expresses the 5-HT7 receptor allowing basal levels of 5-HT to affect the response gain modulation exerted by these LNs upon olfactory projection neurons (PNs)[12]. In another example, repeated exposure to noxious stimuli sensitizes larval nociceptors in *Drosophila* to feedback inhibition mediated by inhibitory 5-HT1A and 1B receptors to enable an experience-dependent reduction in nociceptive responses[13]. Thus, in these examples, uniform expression of a 5-HT receptor allows fine-tuning of the computation implemented by a population of neurons.

However, modulators can have heterogeneous effects on stimulus-driven responses based on the sensory tuning of neurons within a single neuron class[14–16]. This raises the possibility that

[1]Department of Biology, West Virginia University, Morgantown, WV, USA. [2]Department of Biology, Case Western Reserve University, Cleveland, OH, USA. [3]These authors contributed equally: Julius Jonaitis, Mohd F. E. B. Mazri. e-mail: amd358@case.edu

modulatory systems can selectively impact the processing of specific sensory signals, rather than impacting the broad computation subserved by the entire neuron class. For instance, as a population, the ventral and lateral-ventral projection neurons (v-PNs and lv-PNs, respectively) in the AL of *Drosophila* express all five insect 5-HT receptors[17], which differ in binding affinity and second messenger systems coupling[18–20]. Individual v-PNs and lv-PNs innervate different subregions of the olfactory system[21–24], raising the possibility that 5-HT differentially modulates v-PNs and lv-PNs based on the volatile chemicals or odor categories to which they respond. Here, we take advantage of the experimental tractability of *Drosophila* to determine if heterogeneous modulatory receptor expression can reflect the sensory tuning within a neuronal class.

The cholinergic lv-PNs and GABAergic v-PNs, of which there are ~70 per AL[23,25,26], project to the lateral horn (LH)[23,27] which is a second-order olfactory neuropil associated with odor valence coding[28–30]. Although less is known about lv-PNs, v-PNs provide feedforward inhibition to the LH[22,31,32] to refine the spatiotemporal patterns of odor-evoked activity[22,29,32–35] and v-PNs have been implicated in playing a role in odor discrimination[31,34], valence coding[22,32] and habituation[36]. In this study, we found many different patterns of 5-HT receptor co-expression by individual v-PNs and lv-PNs. Stochastic labeling revealed that v-PNs and lv-PNs expressing each 5-HT receptor innervate partially overlapping sets of glomeruli, and photoactivatable GFP (PA-GFP) demonstrated that v-PNs expressing each 5-HT receptor occupy different zones within the lateral horn. Endogenous 5-HT release and 5-HT receptor pharmacology differentially modulate v-PNs projecting to different sub-regions within the AL and LH, and connectomic analysis revealed that these v-PNs synapse upon separate populations of LH neurons. Overall, while the v-PNs play a unified function (odor decorrelation), our results demonstrate that serotonin differentially modulates subsets of neurons within this population that encode distinct odor scenes. Heterogeneous receptor expression may therefore enable nuanced modulation of the computations provided by a single neuron class.

Results

Serotonin receptors are heterogeneously co-expressed by v-PNs and lv-PNs

While v-PNs and lv-PNs collectively express all five 5-HT receptors[17], the organizational principles of 5-HT receptor expression within these populations is unknown. In addition to expressing different transmitters (Supplementary Fig. 1a–c), the v-PNs and lv-PNs synapse upon third-order olfactory neurons that project to relatively distinct brain regions, with v-PNs synapsing more onto neurons projecting to the superior lateral protocerebrum and within the LH, and lv-PNs synapsing onto neurons that project to the superior medial protocerebrum and the medial lobe of the mushroom bodies (Supplementary Fig. 1d–f). Due to these differences in morphology, we analysed v-PNs and lv-PNs separately. We began by determining if v-PNs and lv-PNs co-express 5-HT receptors and if there are any combinations of 5-HT receptors that are frequently observed. To resolve this, we took an intersectional approach, leveraging 5-HT receptor MiMIC T2A Gal4 lines[37] and LexA knock-in lines[38] to make pairwise comparisons of receptor expression. We first assessed whether the v-PNs and lv-PNs expressed within each 5-HT receptor knock-in LexA line matched the expression from the corresponding 5-HT receptor MiMIC T2A-Gal4 line which had been validated in other brain regions (see Methods). Only the 5-HT2B and 5-HT7 LexA knock-in lines had 100% overlap in their v-PN and lv-PN expression patterns with their respective MiMIC T2A Gal4 driver line (Fig. 1a, Supplementary Fig. 1), so we restricted our comparisons to the 5-HT2B and 5-HT7 knock-in LexA lines with the five MiMIC 5-HT receptor T2A lines (Fig. 1a–c). For both the v-PNs and lv-PNs, most of the five 5-HT receptors were co-expressed, except for the 5-HT2A receptor which was not co-expressed with the 5-HT2B or 5-HT7 (Fig. 1d, Supplementary Fig. 1g–x). The 5-HT2A is expressed by the fewest number of v-PNs, so the lack of co-expression may reflect this low level of expression. The v-PNs tended to have slightly higher degree of co-expression of the 5-HT1A receptor with both the 5-HT2B and 5-HT7 receptors (~30% each) relative to the lv-PNs, while the pattern was reversed for co-expression of the 5-HT1B receptor in lv-PNs (~25% for the 5-HT2B and ~40% for the 5-HT7). Thus, the high degree of 5-HT receptor co-expression give 5-HT the potential to exert a heterogeneous impact on the total population of v-PNs and lv-PNs, greater than could be achieved with either non-overlapping patterns of 5-HT receptor expression or a uniform pattern of expression.

v-PNs and lv-PNs expressing different 5-HT receptors project to distinct subregions within the olfactory system

We next sought to determine if v-PNs and lv-PNs expressing specific 5-HT receptors innervated distinct sets of glomeruli within the AL. One possible explanation for the diverse patterns of co-expression that we observed could be that v-PNs and lv-PNs that respond to distinct sets of odors are differentially modulated by 5-HT. If this is the case, PNs that express different 5-HT receptors should innervate distinct patterns of glomeruli or sub-regions of the LH. To determine if differential 5-HT receptor expression by v-PNs and lv-PNs correlates with differences in glomerular innervation, we used the multi-color flip-out (MCFO) technique[39] to stochastically label v-PNs and lv-PNs within the 5-HT receptor MiMIC T2A Gal4 lines (Supplementary Fig. 2a–c). We then

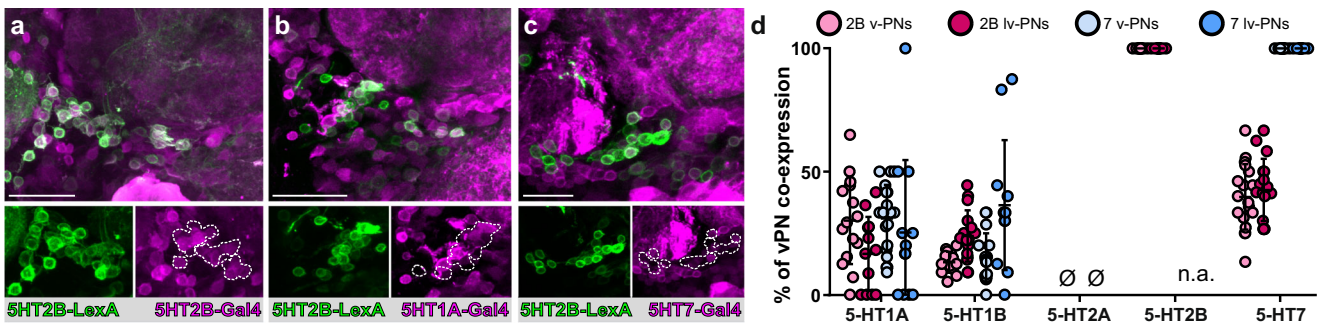

Fig. 1 | As a population v-PNs express a diverse combination of serotonin receptors. a–c Example v-PN cell clusters demonstrating the degree of overlap of expression the 5-HT2B LexA with **a**) the 5-HT2B-T2A-Gal4, **b** the 5-HT1A-T2A-Gal4 and **c** the 5-HT7-T2A-Gal4. **d** Percent of overlap between v-PNs expressed in either the 5-HT2B-LexA (pink) or 5-HT7-LexA (blue) with v-PNs in the T2A Gal4 lines for the other 5-HT receptors ($n = 15$ for 5-HT2B-LexA with 5-HT1A-T2A-Gal4, $n = 14$ for 5-HT2B-LexA with 5-HT1B-T2A-Gal4, $n = 7$ for 5-HT2B-LexA with 5-HT2A-T2A-Gal4, $n = 6$ for 5-HT2B-LexA with 5-HT2B-T2A-Gal4, $n = 19$ for 5-HT2B-LexA with 5-HT7-T2A-Gal4, $n = 19$ for 5-HT7-LexA with 5-HT1A-T2A-Gal4, $n = 16$ for 5-HT7-LexA with 5-HT1B-T2A-Gal4, $n = 7$ for 5-HT7-LexA with 5-HT2A-T2A-Gal4, $n = 13$ for 5-HT7-LexA with 5-HT7-T2A-Gal4). The null sign indicates no observed overlap for the 5-HT2A receptor, and n.a. indicates a redundant receptor co-expression combination that was not tested. Average +/− SEM. All scale bars are 20 μm.

https://doi.org/10.1038/s41467-025-66107-x

scored the glomeruli that v-PNs and lv-PNs from a single animal occupied (Fig.2a) and, as a population, determined the percent of samples in which a given glomerulus was innervated by a v-PN or lv-PN stochastically labeled within a given 5-HT receptor T2A line. Using this approach, we observed that the 5-HT1A, 5-HT1B, 5-HT2A, and 5-HT2B had relatively more overlap compared to v-PNs expressing the 5-HT7 receptor (Fig. 2b). To determine if the patterns of glomerular innervation for the 5-HT7 receptor were dissimilar from the other four receptors, we used hierarchical clustering to group glomerular innervation patterns from individual brains. This analysis revealed that v-PNs and lv-PNs from each 5-HT receptor MiMIC T2A Gal4 generally do not segregate into their own unique clusters (Supplementary Fig. 2d). Instead, two clusters formed, predominantly composed of samples from the 5-HT7 T2A-Gal4 line, whereas the remaining clusters included a mixture of samples derived from the other four 5-HT receptor T2A-Gal4 lines. Overall, this implies that there is a large amount of overlap in glomerular innervation for four of the five 5-HT receptors.

We next asked if v-PNs expressing different 5-HT receptors innervated different regions of the LH. The individual innervation patterns of PNs within the LH are consistent across flies, establishing a zonal map of broad odor categories such as food or pheromone-related odorants[22,32,34,40–46]. We therefore asked whether 5-HT receptor expression could predict the regions of the LH occupied by the axon terminals of v-PNs. We used the T2A-Gal4 lines for the 5-HT1A, 1B, and 7 receptors to drive the expression of photoactivatable-GFP[47] and targeted photostimulation to cell body clusters ventral to the AL (Fig. 3a). After immunolabeling the tissue with a neuropil marker, we characterized the distribution of v-PN processes within the LH. Photoactivation of GFP within v-PNs from each 5-HT receptor T2A-Gal4

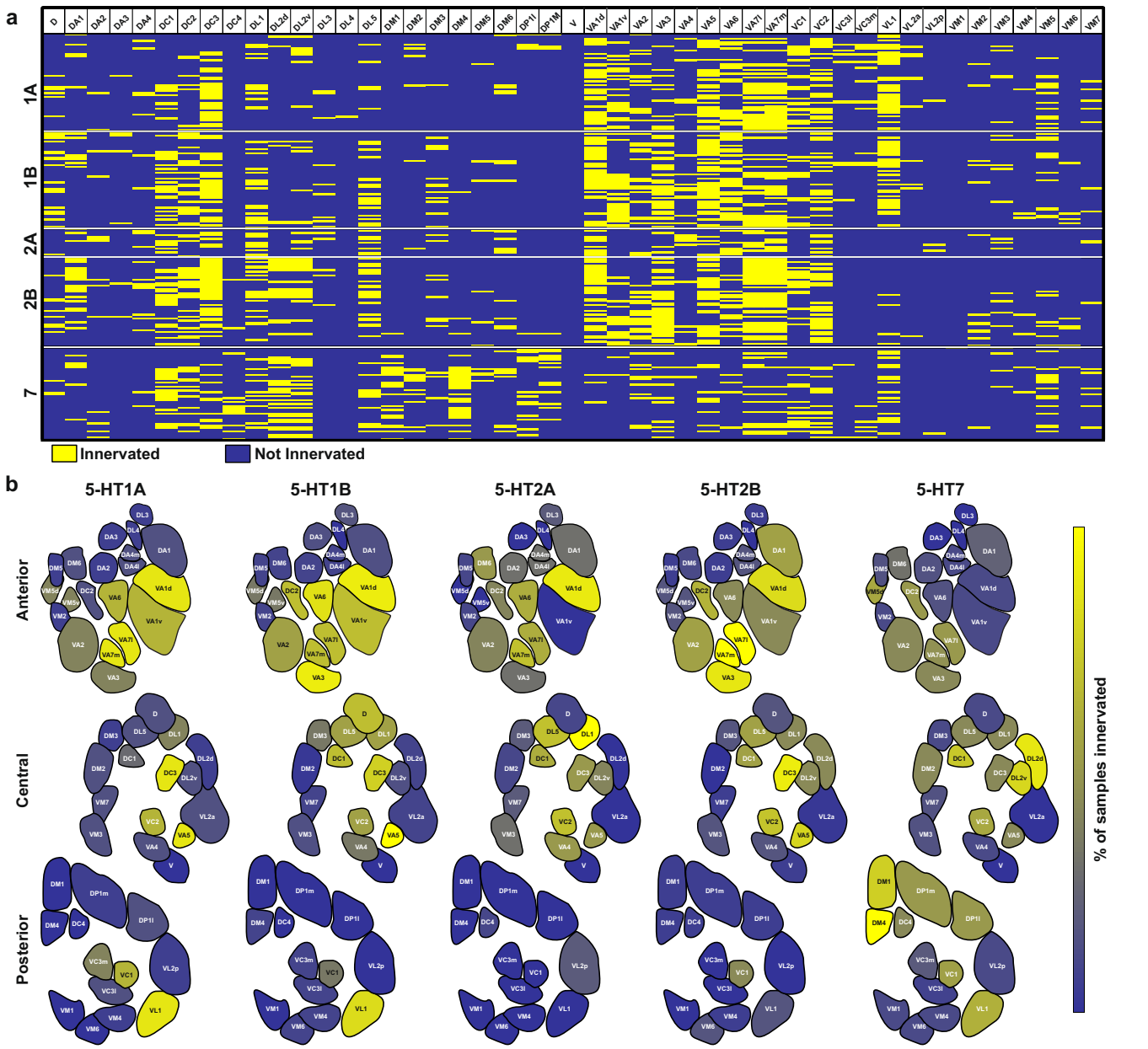

Fig. 2 | Population analysis of v-PN glomerular innervation patterns based on 5-HT receptor expression profile. a Glomerular innervation patterns of v-PNs and lv-PNs stochastically labeled via MCFO using each of the 5-HT receptor T2A-Gal4 lines (5-HT1A, $n = 49$ flies; 5-HT1B, $n = 50$ flies; 5-HT2A, $n = 14$ flies; 5-HT2B, $n = 46$ flies; 5-HT7, $n = 46$ flies). Each row represents the glomeruli innervated by v-PNs in a single AL, with yellow indicating innervation of a given glomerulus and dark blue indicating no innervation. **b** Glomerular maps depicting percent of samples (from 0 to 100%) in which a given glomerulus was innervated by v-PNs stochastically labeled using each of the 5-HT receptor T2A-Gal4 lines.

https://doi.org/10.1038/s41467-025-66107-x

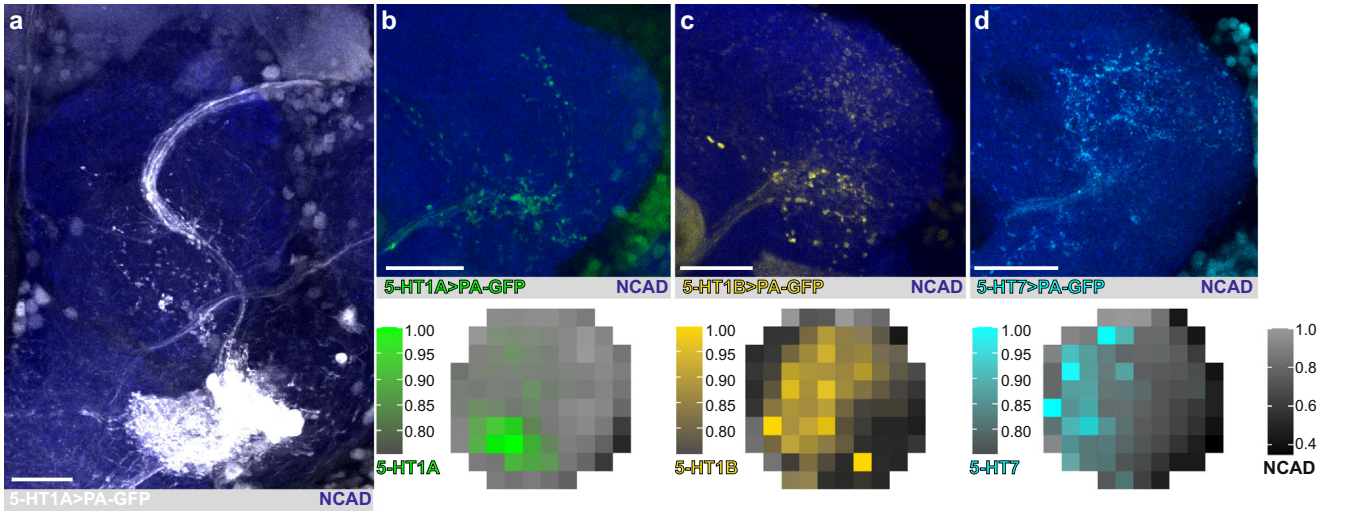

Fig. 3 | v-PNs expressing each 5-HT receptor innervate distinct subregions of the LH. a Example photoactivation of a ventral AL cell body cluster resulting in labeling of v-PNs expressing the 5-HT1A receptor. **b** Example arborization field of 5-HT1A receptor expressing v-PNs (top panel; green) and average intensity (arbitrary units) of LH projections across animals (bottom panel; $n = 5$). **c** Example arborization field of 5-HT1B receptor expressing v-PNs (top panel; yellow) and average intensity (arbitrary units) of LH projections across animals (bottom panel; $n = 7$). **d** Example arborization field of 5-HT7 receptor expressing v-PNs (top panel; cyan) and average intensity (arbitrary units) of LH projections across animals (bottom panel; $n = 5$). Immunolabeling for N-Cadherin (dark blue) highlights LH neuropil in the top panels, and gray shades indicate average NCAD intensity in the bottom panels. All scale bars are 20 μm.

resulted in distinct patterns of LH innervation (ANOVA: $F(2,1265) = 41.46$, $p < 0.0001$) with some degree of overlap, consistent with the amount of 5-HT receptor co-expression (Fig. 1) and glomerular overlap (Fig. 2) observed for v-PNs. The v-PNs expressing the 5-HT1A receptor consistently innervated the ventral and medial portions of the LH (Fig. 3b), whereas v-PNs expressing the 5-HT1B had dense innervation of the ventral LH with diffuse projections extending dorsally (Fig. 3c) (Tukey HSD: $t = 9.48$, $p < 0.0001$). Finally, the v-PNs expressing the 5-HT7 receptor projected dorsally and remaining tightly along the medial margin of the LH (Fig. 3d) which resulted in a pattern that had some overlap with the arborization field of the 5-HT1B expressing v-PNs (Tukey HSD: $t = -1.89$, $p < 0.14$), but very little overlap with the 5-HT1A expressing v-PNs (Tukey HSD: $t = 7.01$, $p < 0.0001$). Thus, while there is overlap in the glomeruli innervated by v-PNs and lv-PNs expressing each 5-HT receptor, v-PNs expressing each 5-HT receptor do innervate different LH zones. This suggests that within the context of the zonal organization of the LH[22,32,34,40–46], 5-HT could differentially impact olfactory processing based on the valence or category associated with an odor.

Differential stimulus-specific modulation of v-PNs is enabled by distinct 5-HT receptor expression

Our next goal was to verify that 5-HT differentially modulates the odor-evoked responses of subsets of v-PNs based on their receptor expression. To achieve this we needed to identify driver lines that met several criteria. The first criteria was that these driver lines needed to exist as both Gal4s and LexAs so that we could use a range of transgenic approaches and should drive expression in predominantly v-PNs within the AL and LH. After an initial screen of the FlyLight database[48], we identified R24H08 and R86G06 as driver lines that met these criteria (Fig. 4a, b, Supplementary Fig. 3). R24H08 included additional neurons expressed within the LH, so we created a splitGal4 line (see Methods) to restrict expression solely to the ~5 v-PNs in this line (Supplementary Fig. 3a, b) for the purposes of visualizing processes in the LH in Ca^{2+} imaging experiments. R24H08 v-PNs densely innervated VC2, DC3, and VL2a (Fig. 4c), whereas the ~5 v-PNs in R86G06 sparsely innervated over 20 glomeruli (Fig. 4d), with only VC2 overlapped with the glomeruli innervated by R24H08. These two sets of v-PNs also innervate distinct regions of the LH, with the R24H08 v-PNs innervating the ventromedial LH (Fig. 4a) and the R86G06 v-PNs innervating the dorsomedial LH (Fig. 4b). Thus, these two sets of v-PNs innervate mostly non-overlapping combinations of AL glomeruli (except for VC2) and LH regions.

The second criterion for the selection of driver lines was that they include v-PNs that all express the same 5-HT receptor. To determine the 5-HT receptors expressed by the v-PNs in each LexA, we first used an intersectional approach with the 5-HT receptor MiMIC T2A Gal4 lines[37] and found that the R24H08 v-PNs exclusively expressed the 5-HT1A and 5-HT1B receptors (Fig. 4e, f, h, Supplementary Fig. 3i–m), whereas the R86G06 v-PNs only expressed the 5-HT7 receptor (Fig. 4g, h, Supplementary Fig. 3n–r). As a secondary form of validation, we performed RNA fluorescent in situ labeling for the predicted 5-HT receptors in each v-PN line using hybridization chain reaction, which revealed that the R24H08 v-PNs express both 5-HT1A and 5-HT1B receptor mRNA (Fig. 4i, j) and the R86G06 v-PNs express 5-HT7 receptor mRNA (Fig. 4k). We could therefore leverage these two driver lines to explore the effects of 5-HT on v-PNs that differ in their 5-HT receptor expression profile.

To identify odorants that activated the v-PNs in each driver line we selected a panel of odors based on the known tuning profiles of OSNs innervating the glomeruli also innervated by these v-PNs[49–53], as well as odor blends such as apple cider vinegar[54] and orange peels[55]. Using this approach, we identified benzaldehyde as an odorant that activated both sets of v-PNs, farnesol as an odorant that only activated R24H08 v-PNs, and 1-octen-3-ol and 1-hexanol as odorants that preferentially activated R86G06 (Fig. 5a, b). We first wanted to determine the effects of endogenous 5-HT on odor-evoked responses of these neurons and selected benzaldehyde, as this odor activates v-PNs in both driver lines. Using a single odorant across both v-PN groups ensured that any differences in the impact of triggering endogenous release of 5-HT would be due to intrinsic differences between R24H08 and R86G06 v-PNs, rather than the AL circuitry activated by different odors. The AL and LH are innervated by a pair of serotonergic neurons called the CSDns (contralaterally-projecting serotonergic deutocerebral neurons)[56–60] which are the sole synaptic source of serotonin within both brain regions[60] and synapse upon each of the principal AL cell classes[61,62]. We therefore used optogenetic activation of the CSDns (Supplementary Fig. 4a, b) while monitoring spontaneous and odor-evoked activity of

https://doi.org/10.1038/s41467-025-66107-x

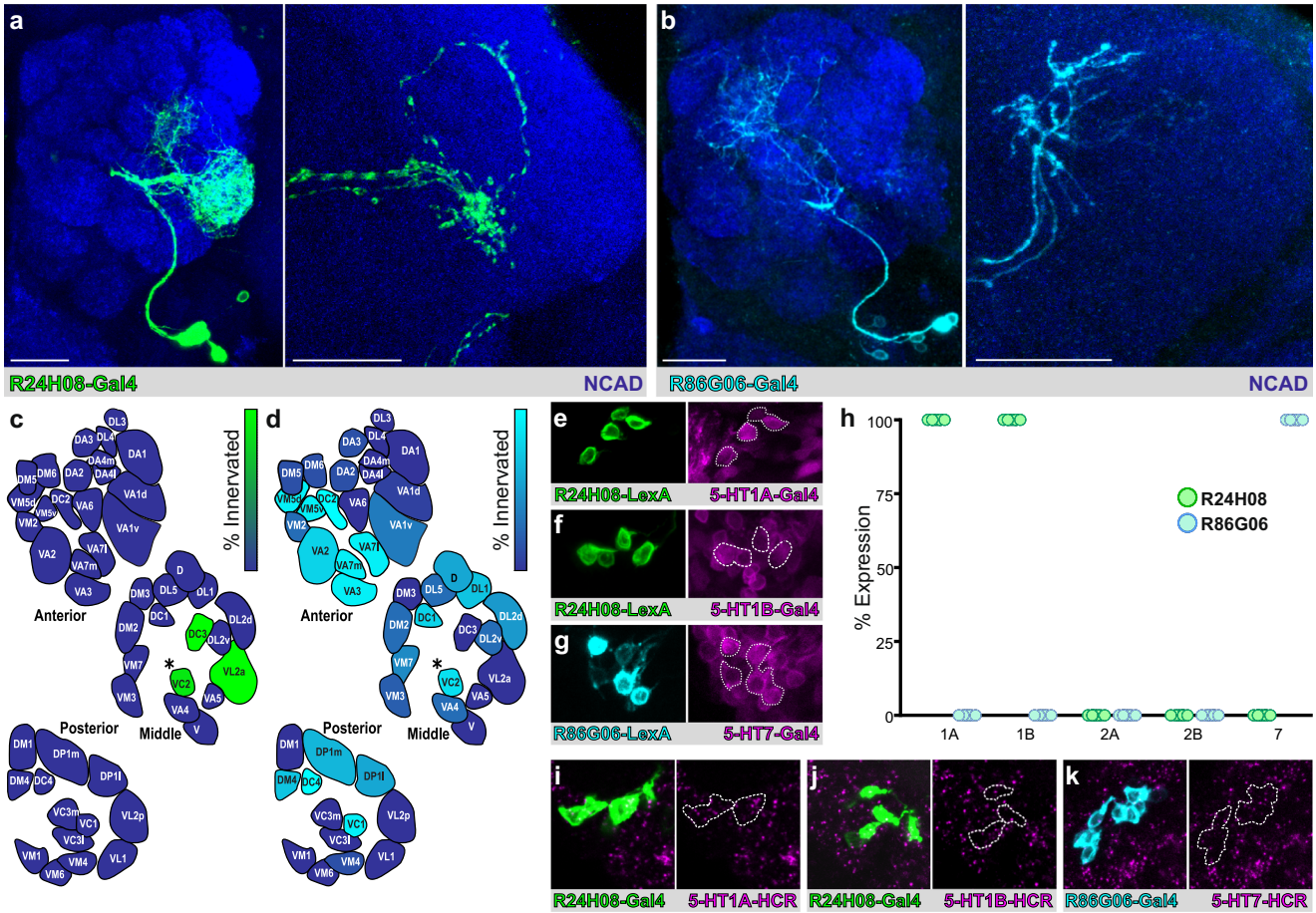

Fig. 4 | v-PNs innervating separate sub-regions of the olfactory system express different 5-HT receptor combinations. Select subsets of v-PNs expressing different serotonin receptors project to distinct regions of the olfactory system. **a** Morphology of the v-PNs within the R24H08 Gal4 (green) within the AL and LH. Immunolabeling for N-Cadherin (dark blue) highlights neuropil. The v-PNs expressed in R24H08 are essentially uniglomerular (except for some sparse branching in other glomeruli), resembling the "mlPN1" type v-PNs[27]. **b** Morphology of the v-PNs within the R86G06 Gal4 (cyan) within the AL and L,H which innervate many glomeruli similar to the "mlPN2" type v-PNs[27]. Note that R86G06 includes OSNs innervating the DC4 glomerulus, so antennae were ablated to obtain images of glomerulus innervation solely by v-PNs in this driver line. **c** Map of glomeruli innervated by R24H08 v-PNs ($n = 18$). **d** Map of glomeruli innervated by R86G06 v-PNs ($n = 14$). An asterisk in (**c**) and (**d**) indicates that VC2 is the only glomerulus innervated by both v-PN driver lines. **e** R24H08 v-PNs overlap with the 5-HT1A-T2A Gal4. **f** R24H08 v-PNs overlap with the 5-HT1B-T2A Gal4. **g** R86G06 v-PNs overlap with the 5-HT7-T2A Gal4. **h** Percent of v-PNs within the R24H08 (green; $n = 12, 9, 8, 13, 11$ for the 5-HT1A, 1B, 2A, 2B and 7 receptors) and R86G06 (cyan; $n = 8, 7, 9, 9, 14$ for the 5-HT1A, 1B, 2A, 2B and 7 receptors) LexAs expressed within each 5-HT receptor T2A-Gal4 line. **i, j** HCR labeling against **i**) 5-HT1A receptor ($n = 8$) and **j**) 5-HT1B receptor ($n = 10$) mRNA (magenta) in the R24H08-Gal4 (green). **k** HCR labeling against 5-HT7 receptor ($n = 14$) mRNA (magenta) in the R86G06-Gal4 (cyan). All scale bars are 20 μm.

v-PNs using 2-photon Ca^{2+} imaging. The 5-HT1A/B receptors suppress adenylate cyclase activity, whereas the 5-HT7 receptor activates adenylate cyclase[20], thus we predicted that activation of the CSDns would enhance the activity of the v-PNs within the R86G06 driver line and reduce the activity of v-PNs in R24H08. Consistent with this prediction, activating the CSDns just prior to odor stimulation nearly doubled the odor-evoked responses of R86G06 v-PNs (Fig. 5c, d), while causing a slight, but non-significant decrease in the amplitude of odor-evoked responses from R24H08 v-PNs (Fig. 5e, f). It should be noted that R24H08 LexA responses to benzaldehyde (Fig. 5b) were weaker relative to R24H08 Gal4 (Fig. 5e) so any inhibitory effects of CSDn activation may have been less apparent in these experiments. Finally, optogenetic activation of the CSDns alone elicited a brief excitatory response from the R86G06 v-PNs, but not from either the R24H08 v-PNs (Supplementary Fig. 4c–f) indicating that endogenously 5-HT differentially modulates the activity of these v-PN subsets.

The extensive synaptic connectivity of the CSDns across the AL and LH[12,60–63] could allow for the effects of 5-HT on odor-evoked responses of v-PNs to arise via polysynaptic mechanisms. To determine the degree to which 5-HT directly modulates v-PNs, we used 5-HT receptor pharmacology to isolate the impact of activating 5-HT receptors directly expressed by each v-PN subset (Fig. 6, Supplementary Fig. 5). Similar to CSDn activation (Fig. 6a, b), the odor-evoked responses of R86G06 v-PNs to 1-octen-3-ol and 1-hexanol were enhanced by both 5-HT and the 5-HT7 receptor agonist AS-19 (Fig. 6e, f). To determine if the enhancement of odor-evoked responses by 5-HT and AS-19 could be attributed to endogenous expression of the 5-HT7 receptor, we drove a 5-HT7 receptor RNAi in the R86G06 driver line. Although R86G06 includes DC4 OSNs, these OSNs do not express the 5-HT7 receptor[17,64]. The 5-HT7 receptor RNAi eliminated the 5-HT induced enhancement of responses to 1-hexanol in R86G06 v-PNs, but not 1-octen-3-ol (Fig. 6e). The odorant-dependent variability in the impact of 5-HT7 RNAi in R86G06 v-PNs is consistent with similar observations for cholinergic PNs in *Drosophila*[65] and other insects[66], and 5-HT has polysynaptic effects on multiglomerular PNs in larval *Drosophila*[63]. We expected that the enhancement of odor-evoked responses by AS-19 would be abolished by expressing the 5-HT7 RNAi, however, AS-19 caused responses to 1-octen-3-ol and 1-hexanol to be significantly reduced (Fig. 6e). This suggests that AS-19 both directly modulates R86G06 v-PNs and enhances inhibitory input to the

https://doi.org/10.1038/s41467-025-66107-x

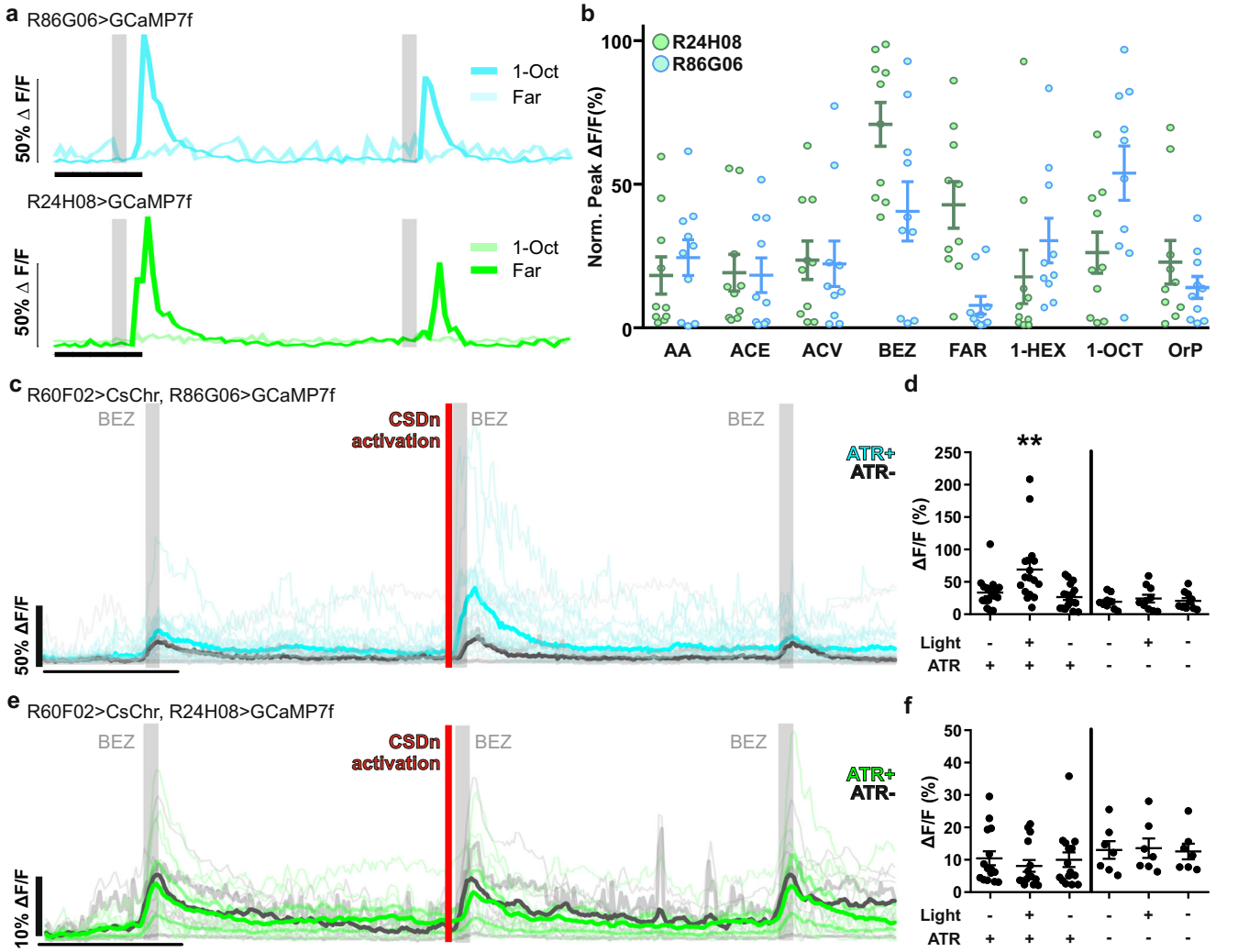

Fig. 5 | Endogenous 5-HT differentially modulates v-PN odor-evoked responses. **a** Example traces recorded from R86G06 v-PNs responding to 1-octen-3-ol, but not farnesol (blue; top panel) and R24H08 v-PNs responding to farnesol, but not 1-octen-3-ol (green; bottom panel). **b** Ca^{2+} imaging responses (peak %dF/F) of R24H08 (green) and R86G06 (cyan) v-PNs to a panel of odors. AA; acetoin acetate, ACE; acetophenone, ACV; apple cider vinegar, BEZ; benzaldehyde, FAR; farnesol, 1-HEX; 1-hexanol, 1-OCT; 1-octen-3-ol, OrP; orange peel ($n = 10$). Average +/− SEM. **c** Optogenetic activation of the CSDns (red bar) via R60F02-Gal4 during odor stimulation of R86G06-LexA v-PNs with benzaldehyde ("BEZ"; gray bars). The cyan trace is the average response recorded from flies fed all-trans retinal (ATR +) and the black trace is the average response from ATR- control flies. **d** Optogenetic activation of the CSDns significantly enhances responses of R86G06 v-PNs to benzaldehyde. Repeated-measures one-way ANOVA followed by Tukey's multiple comparisons test (two-sided), adjusted for multiple comparisons; t = 9.12, $p = 0.0035$ for ATR+ flies ($n = 17$) and $p = 0.3331$ for ATR- flies ($n = 10$). "Light +" indicates odor trial with optogenetic activation of the CSDns, "Light -" indicates odor trials without optogenetic activation of the CSDns. Average +/− SEM. **e** Optogenetic activation of the CSDns (red bar) via R60F02-Gal4 during odor stimulation of R24H08-LexA v-PNs with benzaldehyde ("BEZ"; gray bars). The green trace is the average response recorded from flies fed all-trans retinal (ATR+) and the black trace is the average response from ATR- control flies. **f** Optogenetic activation of the CSDns caused a slight, non-significant decrease in responses of R24H08 v-PNs to benzaldehyde. Friedman test, with Dunn's post-hoc test. $p = 0.305$ for ATR + flies ($n = 16$), and $p = 0.4861$ for ATR- flies ($n = 7$). Average +/− SEM.

R86G06 v-PNs, which is revealed once the direct modulation is blocked. Altogether, these results indicate that the enhancement of R86G06 v-PNs by 5-HT likely arises from a combination of direct and polysynaptic mechanisms.

Since the 5-HT1A and 5-HT1B receptors are negatively coupled to adenylyl cyclase, we expected that 5-HT would have a suppressive effect on the odor-evoked responses of R24H08 v-PNs. However, when recording odor-evoked responses of R24H08 v-PN processes in the LH to farnesol and benzaldehyde, 5-HT and ipsapirone (a 5-HT1A and 5-HT1B agonist) only caused a slight, non-significant reduction (Supplementary Fig. 5c, d). One possible explanation was that bath application of pharmacological agents induced a transient effect on R24H08 v-PNs that dissipated between odor trials. However, bath application of ipsapirone for 8 min did not cause a noticeable change to the baseline fluorescence of R24H08 v-PNs (Supplementary Fig. 5g). Another possible explanation could be that the impact of 5-HT is localized to R24H08 v-PN processes within the AL, rather than the LH as the processes of the R24H08 v-PNs overlap extensively with those of the CSDns in the AL (Supplementary Fig. 5h), but not in the LH (Supplementary Fig. 5i). We therefore repeated the experiments above while imaging in the AL and found that ipsapirone significantly reduced the responses of R24H08 v-PNs to farnesol and benzaldehyde recorded within the AL (Fig. 6d, e). Furthermore, expression of 5-HT1A RNAi in the R24H08 v-PNs eliminated this reduction (Fig. 6f) implying that any suppressive effects of 5-HT on R24H08 v-PNs was due to direct 5-HT1A/B receptor agonism by ipsapirone. Overall, our physiological results are consistent with 5-HT differentially impacting each R86G06 and R24H08 v-PNs due to both direct receptor activation and via polysynaptic modulation of other AL neurons.

https://doi.org/10.1038/s41467-025-66107-x

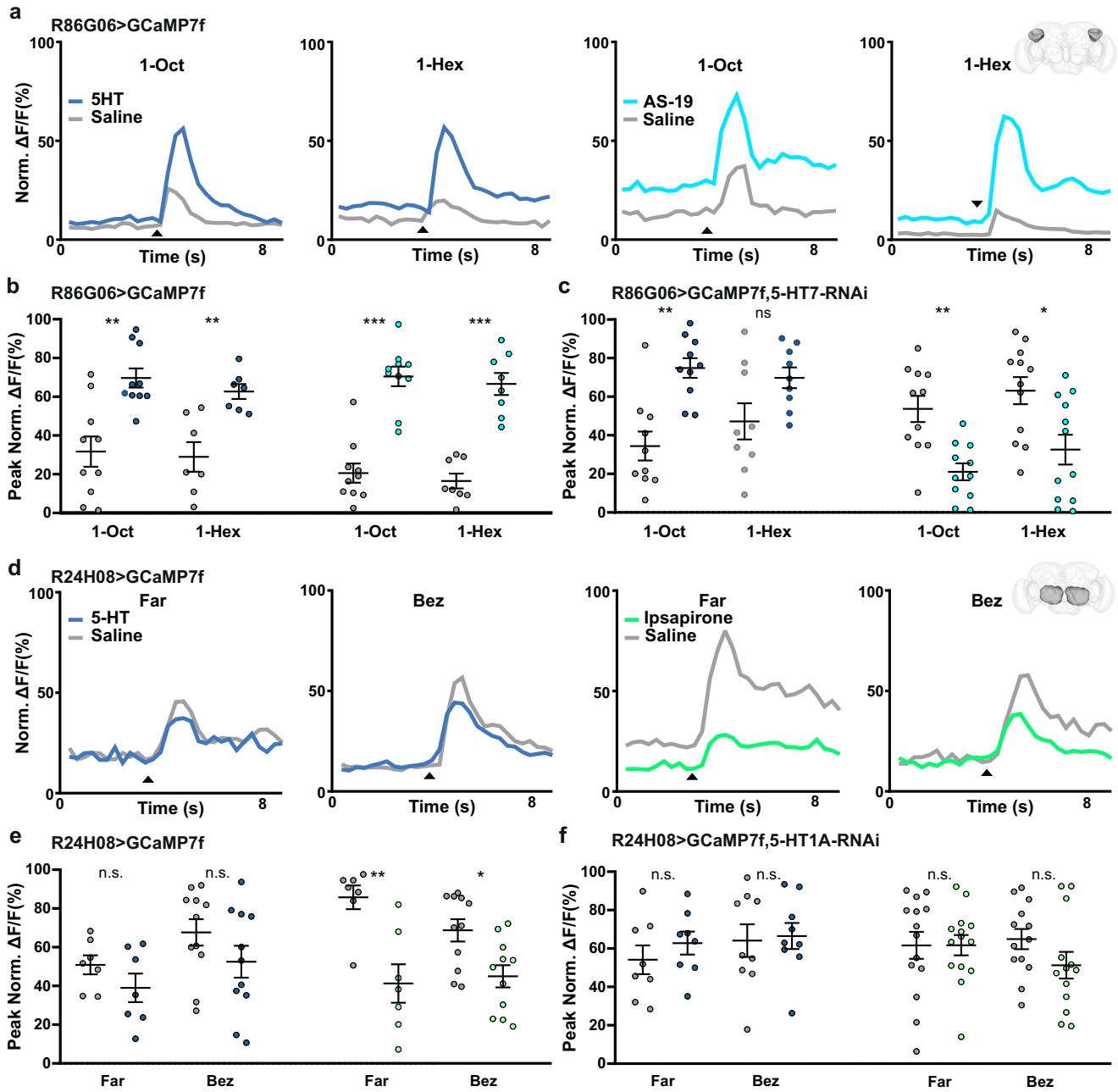

Fig. 6 | Serotonin differentially modulates odor-evoked responses of v-PNs. **a** Average responses of R86G06 v-PNs to 1-octen-3-ol or 1-hexanol before (gray traces) and after application of 5-HT (dark blue) or a 5-HT7 receptor agonist (AS-19; cyan). Arrowhead indicates time of odor application. Traces were recorded from LH processes of the R86G06 v-PNs (indicated by darkened region of brain cartoon) **b** 5-HT and AS-19 enhance odor evoked responses of R86G06 v-PNs. 5-HT, $n = 10$ (1-Oct), $t = 3.60$, $p = 0.0057$; $n = 7$ (1-Hex), $t = 4.256$, $p = 0.0053$; AS-19, $n = 10$ (1-Oct), $t = 5.826$, $p = 0.0003$; $n = 8$ (1-Hex), $t = 6.837$, $p = 0.0002$; 3 repeated stimulations, significance tested using paired samples T-test (two-sided). Average +/− SEM. **c** RNAi knockdown of the 5-HT7 receptor in R86G06 v-PNs results in a loss of 5-HT-induced enhancement of 1-hexanol responses and causes AS-19 to suppress R86G06 v-PN responses. 5-HT, $n = 10$ (1-Oct), $t = 3.677$, $p = 0.0051$; $n = 9$ (1-Hex), $t = 1.937$, n.s.; AS-19, $n = 11$ (1-Oct), $t = 3.707$, $p = 0.0041$; $n = 12$ (1-Hex), $t = 2.449$ $p = 0.0323$; 3 repeated stimulations, significance tested using paired sample T-test (two-sided). All recordings were made from R86G06 v-PN axon terminals in the lateral horn. Average +/− SEM. **d** Average responses of R24H08 v-PNs to farnesol (Far) or benzaldehyde (Bez) before (gray traces) and after application of 5-HT (blue) or a 5-HT1A/1B receptor agonist (Ipsapirone; green). Arrowhead indicates the time of odor application. Traces were recorded from AL processes of the R24H08 v-PNs (indicated by darkened region of brain cartoon) **e** 5-HT does not significantly affect odor-evoked responses of R24H08 v-PNs, while ipsapirone reduces responses. 5-HT, $n = 7$ (Far), $t = 1.376$, n.s., $n = 11$ (Bez), $t = 1.235$, n.s.; Ipsapirone, $n = 7$, (Far), $t = 5.436$, $p = 0.0016$, $n = 11$ (Bez), $t = 2.465$, $p = 0.0334$, 3 repeated stimulations, significance tested using paired sample T-Test (two-sided). Average +/− SEM. **f** RNAi knockdown of the 5-HT1A receptor in R24H08 v-PNs results in a loss of the ipsapirone induced reduction of odor-evoked responses. 5-HT, $n = 8$ (Far), $t = 0.856$ n.s.; $n = 9$ (Bez), $t = 0.181$ n.s.; Ipsapirone, $n = 14$ (Far), $t = 0.007$ n.s.; $n = 13$ (Bez), $t = 1.446$, n.s.; 3 repeated stimulations, significance tested using paired sample T-test. All recordings were made from R24H08 v-PN processes in the AL. Average +/− SEM.

https://doi.org/10.1038/s41467-025-66107-x

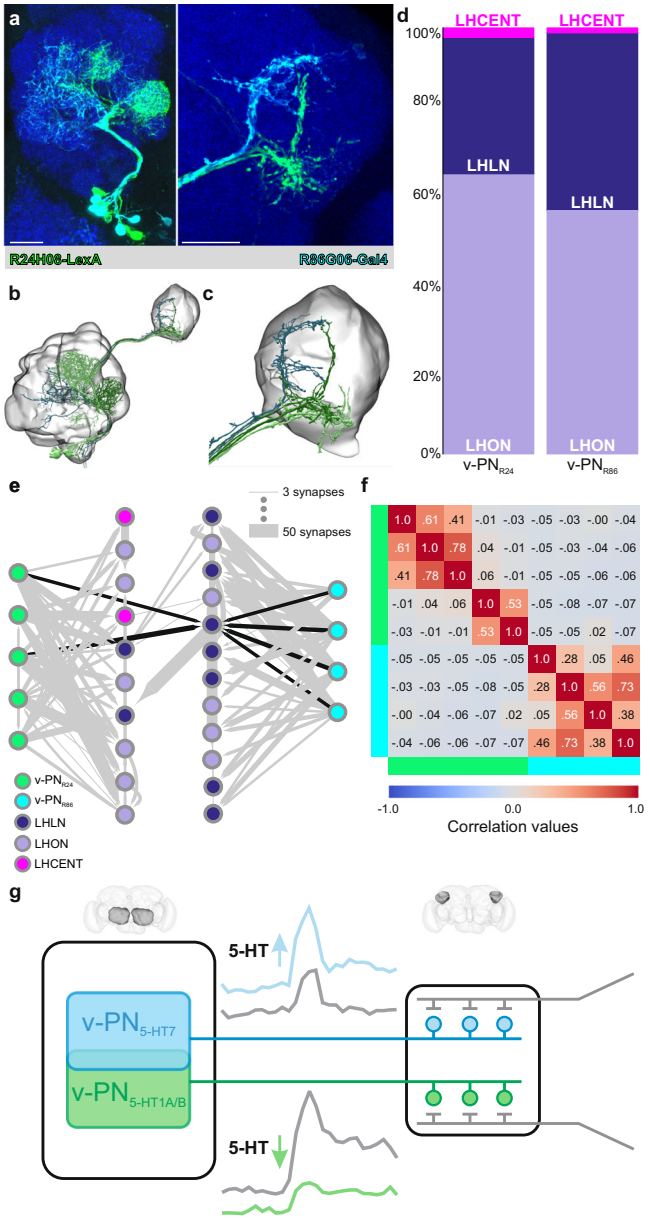

Fig. 7 | v-PNs expressing different 5-HTRs have divergent synaptic partners within the LH. a overlap of AL (left) and LH (right) projections of the R24H08 (green) and R86G06 (cyan) v-PNs. Immunolabeling for N-Cadherin (dark blue) highlights neuropil. All scale bars = 20 μm. **b** Reconstruction of the v-PNs from the Hemibrain dataset that most closely resemble the R24H08 (v-PN$_{R24}$; green) and R86G06 (v-PN$_{R86}$; cyan) driver lines within AL and LH volumes. R24H08 v-PNs are shown in two shades of green to highlight the v-PNs predominantly innervating the VL2a glomerulus (dark green) and the DC3 glomerulus (light green). **c** Reconstruction of the axon terminals of the two v-PN groups within the LH. **d** Synapse fractions of the downstream LH neurons targeted by the candidate v-PNs from the R24H08 and R86G06 driver lines. LH output neurons (LHONs; lavender), LH local neurons (LHLNs; purple), LH centrifugal neurons (LHCENTs; pink). **e** Graph plot of the downstream synaptic targets of the v-PN$_{R24}$ (green) and v-PN$_{R86}$ (cyan) shows very little convergence, except for a single LHLN that is targeted by two v-PN$_{R24}$ and all four v-PN$_{R86}$ (black arrows). **f** Correlation matrix for the downstream partners of each v-PN$_{R24}$ and v-PN$_{R86}$ in the LH. Correlation values range between -1.0 (blue) and 1.0 (red). Green bar indicates individual v-PN$_{R24}$ and blue bar indicates individual v-PN$_{R86}$. The individual HemiBrain IDs used from top to bottom and left to right are 5813077810, 948834414, 1889883818, 1857143769, 1415825344, 791298858, 760264077, 729219639 and 698526273. **g** Schematic proposed model for the role of 5-HT in modulating v-PNs. v-PNs that express different 5-HT receptors (green = 5-HT1A/B, blue = 5-HT7) innervate partially overlapping combinations of glomeruli (left side, antennal lobes highlighted gray in brain reconstruction), thus participating in responses to partially overlapping sets of odors. v-PNs that express different 5-HT receptors project to different regions within the lateral horn (right side, lateral horns highlighted gray in brain reconstruction) and synapse upon different sets of lateral horn neurons (gray neurons within lateral horn). We propose that this enables 5-HT to differentially modulate (gray traces indicate before 5-HT, green/blue traces indicate effects of 5-HT) feedforward inhibition provided to separate output paths from the lateral horn. Brain meshes highlighting the antennal lobes and lateral horns were generated from the FAFB dataset[26] on FlyWire[25,113].

v-PNs expressing different 5-HT receptors diverge in their downstream target

Our final question was do v-PNs expressing different 5-HT receptors converge upon the same downstream targets? Theoretically, third order olfactory neurons within the lateral horn could integrate synaptic input from v-PNs differentially modulated by 5-HT, allowing serotonergic modulation to shift which odor-evoked responses have the greatest impact on a common partner. Alternatively, v-PNs that express different 5-HT receptors could synapse on non-overlapping populations so that the impact of serotonergic modulation on each set of v-PNs remains separate. To address this question, we turned to the hemibrain dataset[67], a nanoscale resolution electron microscopy (EM) volume that includes the right AL and LH of a female *Drosophila*. By querying v-PNs in hemibrain based on the AL glomerular innervation patterns and branching patterns within the LH observed for the R24H08 and R86G06 driver lines (Fig. 7a), we identified five and four v-PNs within the EM dataset that closely resembled the v-PNs expressed by the R24H08-Gal4 and the R86G06-Gal4 lines, respectively (referred to as v-PN$_{R24}$ and v-PN$_{R86}$; Fig. 7b, c and Table 3). In particular the branching patterns of the v-PNs within the LH of the EM dataset (Fig. 7c) were very similar to that observed from light microscopy data (Fig. 7a). To determine if these two groups of v-PNs synapse upon similar neuronal demographics within the LH, we queried all of the downstream partners of the nine v-PNs and classified each downstream partner within the LH as an LH output neuron (LHON), LH centrifugal neuron (LHCENT), or LH local neuron (LHLN) based on the cell body tract to which they belong, and the relative distribution of presynaptic and postsynaptic sites within the LH and other brain regions, as described previously[68,69]. The proportions of these LH neuron types targeted by each v-PN group were very similar (Fig. 7d), with both primarily targeting LHONs, a smaller proportion of LHLNs and very few LHCENTs. We then searched for all downstream partners that receive convergent synaptic input from 2 or more of the nine total v-PNs (i.e. combining all v-PN$_{R24}$ and v-PN$_{R86}$). Of the 22 total lateral horn neurons (see Table 3) that receive convergent input from two or more of the queried v-PNs, only 1 LHLN was downstream of both v-PN$_{R24}$ and v-PN$_{R86}$ (Fig. 7e). Thus, while the two groups of v-PNs target similar neuron-class demographics, there was very little convergence in the downstream neuronal populations targeted by v-PNs that express different 5-HT receptors (Fig. 7e). A cross correlational analysis of all downstream partners of the v-PN$_{R24}$ and v-PN$_{R86}$ revealed that the downstream connectivity of the individual v-PN$_{R24}$ and v-PN$_{R86}$ were highly correlated within each subgroup, while there was no correlation between the two v-PN subgroups (Fig. 7f). This implies that, at the level of the LH, the impact of 5-HT on v-PNs that express different 5-HT receptors remains segregated.

Overall, this approach suggests that v-PNs with distinct 5-HT receptor expression patterns innervate partially overlapping combinations of glomeruli, yet different regions within the LH and synapse upon different third-order neurons. Given this framework, 5-HT is poised to differentially modulate v-PN and lv-PN sub-populations to adjust distinct components of odor representations, rather than uniformly up- or downregulate responses across the entire population (Fig. 7g).

Discussion

Each neuronal class within any sensory network supports distinct computations; however, the relative importance of each computation can be modified based on recent network activity or the current physiological needs of the individual animal. Frequently, neurons within a given neuronal class uniformly express one or a few modulatory receptors, enabling a neuromodulator to adjust the specific computation that they support. For instance, different cell types within the optic lobe of *Drosophila* express different 5-HT receptors[70] and play distinct roles in sensory processing[71], suggesting that 5-HT differentially affects individual computations supported by the visual system. We demonstrate that even within a single cell class there can be differential receptor expression allowing a modulator to prioritize the responses of some neurons over others. We first found that there is extensive, heterogeneous 5-HT receptor co-expression within the v-PN population and that v-PNs that express each 5-HT receptor project to different regions within the AL and LH. We demonstrate that differential receptor expression results in 5-HT enhancing the responses of some v-PNs while reducing the responses of others, although 5-HT likely also impacts responses via polysynaptic interactions (Figs. 5, 6). Finally, we show that the v-PNs with distinct 5-HT receptor expression synapse upon different third-order neurons within the LH. In the olfactory system of *Drosophila*, serotonergic neurons interact with most principal neuron classes[60,61] to impact olfactory processing and behavior[62,72–74]. To this end, the diverse suite of serotonin receptors expressed by each neuronal class provides precise regulation of distinct computations so that network activity can be contextually optimized[75–77]. In this study, we demonstrate that even within a neuronal class there can exist combinatorial receptor expression allowing a single modulator to differentially impact sensory-driven responses.

The v-PNs not only expressed all five 5-HT receptors, but also had extensive co-expression of 5-HT receptors, potentially resulting in diverse effects on odor coding. A diverse set of receptors provides the nervous system with a great deal of flexibility for regulating the activity of individual cellular components within a network. A single signaling molecule such as 5-HT can have a range of effects as 5-HT receptors differ in their threshold for activation, time course of action, and the valence of their impact on neuronal activity. The half-effective concentrations of 5-HT for *Drosophila* 5-HT receptors differ over a range of two orders of magnitude[18]. Collectively 5-HT receptors couple with G_s, G_q and G_i allowing for activation of a range of transduction mechanisms with different degrees of potential amplification[19,20]. Finally, 5-HT receptors can be restricted to specific neuronal compartments[78] which would allow spatial control over the effects of this modulator based on the neuropil, which would be consistent with our observation that the effects of 5-HT and 5-HT receptor agonists were most potent when recording from R24H08 v-PN processes within the AL (Fig. 6). We report that not only are all five 5-HT receptors expressed by v-PNs, but that there is extensive co-expression of 5-HT receptors (Fig. 1). Although we could not test all pairwise combinations, v-PNs and lv-PNs have some degree of co-expression for receptors that couple to different second messenger pathways. For instance, the 5-HT2B receptor (which couples to IP_3 pathways) is co-expressed with both 5-HT1 receptor subtypes and the 5-HT7 receptor (all three of which impact adenylyl cyclase). Furthermore, co-expression of the 5-HT7 receptor (which positively couples to adenylyl cyclase via G_s) and the 5-HT1 receptors (which negatively couple to adenylyl cyclase via G_i) indicates that there is integration within even a single second messenger pathway. Co-expression effectively increases the potential effects of 5-HT from the singular actions of each individual receptor to the wider range of effects endowed by combinatorial patterns of receptor expression. There is also the possibility that 5-HT may have synergistic effects on v-PNs or lv-PNs due to the formation of 5-HT receptor heterodimers[79,80]). For instance, 5-HT1A receptor-induced GPCR inward rectifying potassium (GIRK) channel currents are reduced when cells co-express the 5-HT7 receptor, even though the 5-HT7 receptor does not itself target GIRK[81]. Thus, co-expression of 5-HT receptors can result in interactions between receptors and convergence of downstream transduction pathways.

Neuromodulation provides the nervous system with the ability to regulate the impact that specific neuron classes have on sensory coding. The heterogeneous nature of 5-HT receptor expression by v-PNs and lv-PNs reveals that the modulation of their roles in olfactory coding is more complex than merely up- or down regulating their cumulative impact. As a population, v-PNs and lv-PNs shape innate odor-driven behavior by impacting odor representations in the LH. In a recent study on directional processing of odor information, lv-PNs responsive to the pheromone cis-vaccenyl acetate were shown to play a critical role in promoting copulation rate and male-male aggression[82]. The GABAergic v-PNs have received far more attention than the lv-PNs for their role in refining odor representations in the LH of *Drosophila* and appear to play an important role in odor decorrelation in support of innate and learned odor-guided behavior[22,31,32,83,84]. Long-range inhibition between processing stages as a means to refine odor coding appears to be a conserved feature of the olfactory system across taxa. GABAergic corticobulbar projections support decorrelation of tufted cell odor-evoked responses in mammals[85] similar to the impact of v-PNs on glutamatergic LH neurons in *Drosophila*[83]. Furthermore, inhibition of mammalian GABAergic corticobulbar projections[85] and inhibition of the neurons expressed in the Mz699 Gal4 line in *Drosophila*[31] reduces odor discrimination in behavioral assays, demonstrating a role for long-range inhibitory projections in fine odor coding. Glutamatergic corticobulbar feedback on the other hand, decorrelates mitral cell odor representations via disynaptic inhibition[86,87] and thus may play a complementary role to GABAergic corticobulbar feedback in mammals. Our data suggests that the impact of v-PNs and lv-PNs on refining odor representations are non-uniformly modulated by 5-HT. In addition to heterogeneous 5-HT receptor expression within both populations (Fig. 1), v-PNs and lv-PNs expressing different 5-HT receptors occupy distinct subsets of glomeruli (Fig. 2) and project to distinct zones within the LH (Fig. 3). The odor-tuning of specific PNs supports their participation with the coding of distinct "odor scenes"[33,83], and thus 5-HT may differentially affect the processing of specific odor combinations. Furthermore, the zonal organization of the LH[22,44,46,88] and the projections of each lv-PN and v-PN into these zones may reflect distinct roles in coding of distinct stimulus features such as valence, identity or intensity[22,28,29,83]. Within the AL, the R24H08 v-PNs densely innervate the DC3 and VL2a glomeruli, both of which respond to plant derived odors associated with reproductive success[49,89,90], and project to the ventral LH which is associated with the processing of pheromonal odorants[44,46]. Our physiological results (Figs. 5, 6) demonstrate that 5-HT suppresses their activity while simultaneously enhancing the responses of R86G06 v-PNs that process odors with a different behavior context. Furthermore, both R24H08 and R86G06 v-PNs respond to benzaldehyde, an odorant that is repellent to flies[51,91], yet 5-HT differentially impacts the odor-evoked responses of each v-PN type. This demonstrates that 5-HT can differentially modulate individual neurons participating in the representation of the same stimulus. The divergence in synaptic targets of these two v-PN groups suggests that separate streams of odor information may also be differentially modulated. Consistent with this, knockdown of the 5-HT1A and 1B receptor (but not the 5-HT7 receptor) in v-PNs blocks experience dependent plasticity in odor evoked responses[84]. Future work will need to focus on the behavioral consequences of differential modulation of v-PNs by 5-HT by implementing a wide range of assays that probe ecological context, locomotor strategy and hedonic valence.

Within cell-class diversity of receptor expression adds a layer of nuance to our understanding of neuromodulation of sensory processing. It is difficult to determine how many neuron classes are present

within a network[92] and heterogeneity within a cell class can blur the lines between functional categories[93,94]. For instance, insulin-producing cells in *Drosophila* heterogeneously express a diverse set of modulatory receptors, allowing individual endocrine cells to be differentially regulated from each other[95]. In our case, the diversity of 5-HT receptor expression patterns within the lv-PNs and v-PNs may merely reflect functional subdivisions within the two populations. The v-PNs consist of at least three morphological classes (uniglomerular, multiglomerular and panglomerular[27]) and there may be other biophysical or molecular properties that underlie additional functional subdivisions. Within cell-class diversity is rife within the AL LNs[24,96–104], so it is not difficult to imagine that similar diversity may exist for v-PNs and lv-PNs. The consequences of within cell class diversity for neuromodulation can be seen even in examples in which only one modulatory receptor is expressed. In *Drosophila*, only a subset of OSN types express the inhibitory receptor for the neuropeptide MIP, allowing this modulator to reduce odor-evoked responses in some glomeruli via direct inhibition and enhance responses in other glomeruli via disinhibition[14]. The intrinsic diversity of AL neuron classes and the diversity of all modulatory receptors[59,102], could therefore provide a large parameter space within which odor coding can be fine-tuned within a variety of contexts.

Methods

Fly stocks

All fly stocks were raised on a standard cornmeal/agar/yeast medium at 24 °C on a 12:12 light/dark cycle at ~60% humidity. The 5-HT receptor MiMIC T2A Gal4 lines[37] have been used to study 5-HT receptor expression in several contexts in *Drosophila*. Single cell RNA sequencing of neurons in the visual system has been used to validate predictions made with these 5-HT receptor MiMIC T2A Gal4 lines[70] and within the olfactory system, our prior work using these reporters predicted that OSNs express the 5-HT2B receptor[17] which was corroborated by subsequent scRNAseq antennal datasets[64]. Male and female flies aged 2-7 days post-eclosion were used for all experiments. All fly stocks used are listed in Table 1 and genotypes of flies used to generate each figure panel are listed in Table 2.

Immunocytochemistry and image acquisition. All antibody information is listed in Table 1. Immunocytochemistry and image acquisition was performed as described previously[17,60]. Briefly, brains were dissected in *Drosophila* External Saline (CSHL recipe) for 30 min and placed in 4% paraformaldehyde solution at 4 °C, washed in PBS with 0.5% Triton-X (PBST), incubated in blocking solution which consisted of 4% IgG-free BSA (Jackson ImmunoResearch, CAS:001-000-162) in PBST and incubated for 48 hours in primary antibodies in 4% BSA in PBST with 5 mM sodium azide (PBSAT). Brains were then washed and blocked as above, and incubated for 48 hours in secondary antibodies in 4% BSA in PBSAT. Finally, brains were washed twice with PBST, twice with PBS, run through an ascending glycerol series (40%, 60%, and 80% glycerol in water, respectively), and mounted in VectaShield (Vector Labs, Burlingame, CA #H-1000). Brains were scanned using an Olympus confocal microscope FV1000 equipped with 40x silicon oil immersion lens. Images were viewed and analyzed using Olympus FluoView software (FV10-ASW 4.2 viewer) and processed using Inkscape and CorelDRAW vector quality graphics software. For images of the AL projections of the v-PNs included in the R86G06 driver line, the antennae were ablated 3 days prior to immunolabeling. This eliminated DC4 OSN axons that occluded the dendritic projections of the v-PNs included in this line, allowing for scoring of the glomeruli innervated by these v-PNs.

For MCFO experiments, animals were exposed to different intervals of heat shock to obtain sparse expression of v-PN clones from each 5-HT T2A Gal4 line (0min for 5-HT1A, 5-HT1B, and 5-HT2A, 0, 5, and 10min for 5-HT2B, and 10min for 5-HT7) and were dissected 2-7 days later. Due to strong 5-HT2B-T2A-Gal4 expression in OSNs[17] and 5-HT7-T2A-Gal4 in Johnston's Organ neurons, antennal and maxillary palp ablations were conducted two days before heat shock to prevent obstruction of v-PN processes in the AL or v-PN cell bodies near the AMMC, respectively. Ablations were performed in 3-5 day old flies to ensure loss of OSNs did not affect development of v-PN morphology. MCFO scans could include either only lv-PNs, only v-PNs, or both and if multiple v-PNs and/or vl-PNs were flipped out, their glomerular innervation patterns were grouped for consideration in one sample. We used the coupon collector's problem[105,106] to determine the number of ALs to image based on v-PN counts previously reported for each 5-HT receptor[17]. Any samples in which AL neurons other than v-PNs and lv-PNs were labeled were discarded to avoid misattributing glomerular innervation. The v-PNs and lv-PNs could be distinguished as lv-PN cell bodies enter the AL through an "arched-shape" fascicle that is located posterior to the "S-shaped" fascicle through which the v-PNs enter the AL[24,82]. These fascicles were also used to identify v-PNs and lv-PNs for the co-expression experiments in Fig. 1 and the fascicles are visible using reporters lines for their respective transmitters; a glutamic acid decarboxylase 1 (GAD1) Trojan T2A LexA and a choline acetyltransferase (ChAT) Trojan T2A Gal4 line[107] (Supplementary Fig. 1a–c).

Scans of brains for the MCFO analysis were selected for inclusion if they contain unobstructed views of v-PN cell bodies with their respective morphology and clear glomeruli innervation that could be traced back to an AL fascicle and exiting tract (mALT for lv-PN and mlALT for v-PN). We can only claim that this approach included v-PNs that were most likely to be expressed using MCFO and likely does not represent the total population of v-PNs that express a given 5-HT receptor. We looked at innervation patterns across 47 glomeruli (DA4l and DA4m, VM5d and VM5v, and VAlm and VA1l were each merged), comparing across several established glomerular maps[24,108–110]. If more than one v-PN or lv-PN could be visualized in a preparation, the glomerular innervation for all neurons were included for the single sample, rather than trying to distinguish the innervation patterns of the individual neurons. We more frequently observed lv-PNs for the 5-HT1A (70% of samples), 5-HT1B (94% of samples), 5-HT2A (100% of samples), and 5-HT2B (96% of samples) T2A-Gal4 lines, while we were more likely to observe v-PNs for the 5-HT7 T2A-Gal4 line (96% of samples).

Hybridization chain reaction (HCR)

All supplies for HCR were purchased from Molecular Instruments Inc. (Los Angeles, CA). Brains were dissected in PBS and fixed in 4% paraformaldehyde for 30 minutes at RT. Brains were then run through a series of 15-minute PBST (with 1% Triton x100) washes as mentioned previously. Brains were then pre-hybridized in hybridization buffer for 30 minutes at 37 °C. Afterwards, the hybridization buffer was switched out with a probe solution (4 μl of each probe set per 1000 μl of hybridization buffer) and brains were incubated overnight at 37 °C. The following day, brains were then run through a series of washes with probe wash at 37 °C. This was followed by a series of washes with 5x SSCT at RT. Brains were then pre-amplified in amplification buffer for 30 minutes at RT. While being pre-amplified, 10 μl aliquots of 3 μM hairpin stock solutions were snap-cooled in a thermocycler (Bio-Rad T100 Thermal Cycler). The aliquots were heated for 90 seconds at 95 °C and then removed to cool to RT in a dark drawer for 30 minutes. A hairpin solution was then prepared by adding the snap-cooled aliquots (10 μl per 500 μl of needed solution) to the amplification buffer. This solution was then applied to brains, and they were incubated overnight in the dark at RT. On the third and final day, the brains were run through a series of washes (2 × 5 min, 2×30 min, 2×5 min) with 5x SSCT at RT followed by a series of 10-minute glycerol washes (40%, 60%, 80%). The brains were then mounted and scanned as described above.

Table 1 | Key Resources and Reagents

Reagent Type (species) or resource	Designation	Source or reference	Identifiers	Additional Information
Genetic reagent (*D. melanogaster*)	y^1w^*;5-HT1A-T2A-GAL4MI^{04464}/CyO;	37	N/A	Kind gift from Herman Dierick
Genetic reagent (*D. melanogaster*)	y^1w^*;5-HT1B-T2A-GAL4MI^{05213}/CyO;	37	N/A	Kind gift from Herman Dierick
Genetic reagent (*D. melanogaster*)	y^1w^*;;5-HT2A-T2A-GAL4MI^{00459}/TM6c	37	N/A	Kind gift from Herman Dierick
Genetic reagent (*D. melanogaster*)	y^1w^*:;5-HT2B-T2A-GAL4MI^{05208}/TM3	37	N/A	Kind gift from Herman Dierick
Genetic reagent (*D. melanogaster*)	y^1w^*;5-HT7-GAL4MI^{00215}/TM6C	37	N/A	Kind gift from Herman Dierick
Genetic reagent (*D. melanogaster*)	10XUAS-IVS-mCD8::RFP}attP18,P{y[+t7.7] w[+mC]=13XLexAop2-mCD8::GFP} su(Hw)attP8;;	117	BDSC; 32229 RRID:BDSC_32229	
Genetic reagent (*D. melanogaster*)	w[*]; 10XUAS-IVS-mCD8::GFP}attP40;	117	BDSC; 32186 RRID:BDSC_32186	
Genetic reagent (*D. melanogaster*)	y w*; lexAop RFP-UAS GFP/CyO; TM3/TM6B	Bloomington Drosophila Stock Center	BDSC; 67093 RRID:BDSC_67093	
Genetic reagent (*D. melanogaster*)	hsFlp;;MCFO	39	BDSC; 64085 RRID;BDSC_64085	
Genetic reagent (*D. melanogaster*)	;;40XUAS-IVS-mCD8::GFP	117	BDSC; 32195 RRID;BDSC_32195	
Genetic reagent (*D. melanogaster*)	pJFRC59-13XLexAop2-IVS-myr::GFP	118	Janelia Fly store; 1117286	
Genetic reagent (*D. melanogaster*)	R24H08-GAL4	48	BDSC; 49100 RRID;BDSC_49100	
Genetic reagent (*D. melanogaster*)	R24H08-LexA	48	BDSC; 52732 RRID;BDSC_52732	
Genetic reagent (*D. melanogaster*)	R86G06-GAL4	48	BDSC; 93199 RRID;BDSC_93199	
Genetic reagent (*D. melanogaster*)	R86G06-LexA	48	BDSC; 54990 RRID;BDSC_54990	
Genetic reagent (*D. melanogaster*)	R24H08-p65.AD/CyO; R53F03-GAL4.DBD	119	BDSC; 68845 RRID;BDSC_68301	
Genetic reagent (*D. melanogaster*)	VT046303-Gal4.DBD	120	BDSC; 74970 RRID;BDSC_74612	
Genetic reagent (*D. melanogaster*)	R60F02-Gal4	48	BDSC; 48228 RRID;BDSC_48228	
Genetic reagent (*D. melanogaster*)	10XUAS-IVS-mCD8::RFP}attP18,P{y[+t7.7] w[+mC]=13XLexAop2-mCD8::GFP} su(Hw)attP8;;	117	BDSC; 32229 RRID:BDSC_32229	
Genetic reagent (*D. melanogaster*)	ChAT-Trojan-LexA	107	BDSC; 60317 RRID:BDSC_60317	
Genetic reagent (*D. melanogaster*)	GAD1-Trojan-LexA	107	BDSC; 60324 RRID:BDSC_60314	
Genetic reagent (*D. melanogaster*)	;;Mz699-Gal4	121	N/A	Kind gift from Tzumin Lee
Genetic reagent (*D. melanogaster*)	20XUAS-IVS-Syn21-jGCaMP7b-p10 in su(Hw)attP5	122	BDSC; 80907 RRID:BDSC_80907	
Genetic reagent (*D. melanogaster*)	w*; PBac{y[+mDint2] w[+mC]=20XUAS-IVS-jGCaMP7f}VK00005	122	BDSC; 79031 RRID:BDSC_79031	
Genetic reagent (*D. melanogaster*)	w[1118];P{13xLexAop2-IVS-GCaMP6s-SV40} su(Hw)attP5	118	BDSC; 44589 RRID:BDSC_44589	
Genetic reagent (*D. melanogaster*)	w[1118]; P{y[+t7.7] w[+mC]=GMR60F02-GAL4}attP2	48	BDSC; 48228 RRID:BDSC_48228	
Genetic reagent (*D. melanogaster*)	y[1] v[1]; P{y[+t7.7] v[+t1.8]=TRiP.JF01852}attP2	123	BDSC; 25834 RRID:BDSC_25834	
Genetic reagent (*D. melanogaster*)	y[1] v[1]; P{y[+t7.7] v[+t1.8]=TRiP.JF02576}attP2	123	BDSC; 27273 RRID:BDSC_27273	
Genetic reagent (*D. melanogaster*)	w*;UAS-C3PA,MBdsRed/CyO;MKRS/TM6B	47	N/A	Kind gift from Dr. Marco Gallio
Antibody	Rabbit anti-RFP (1:500 dilution)	Rockland; 600-401-379	RRID: AB_2209751	
Antibody	Chicken anti-GFP (1:500 dilution)	Abcam; ab13970	RRID: AB_300798	
Antibody	Rat anti-NCAD (1:250 dilution)	DSHB; DN-Ex #8	RRID: AB_528121	

Table 1 (continued) | Key Resources and Reagents

Reagent Type (species) or resource	Designation	Source or reference	Identifiers	Additional Information
Antibody	Rabbit anti-hemaglutinin (1:300 dilution)	CST; #3724	RRID: AB_1549585	
Antibody	Mouse anti-V5 (1:500 dilution)	Bio-Rad; # MCA1360D550GA	RRID: AB_2687576	
Antibody	Rabbit anti-GABA (1:500 dilution)	Sigma; A2052	RRID: AB_477652	
Antibody	Rabbit anti-serotonin (1:5,000 dilution)	Immunostar; 20080	RRID: AB_572263	
Antibody	Donkey anti-chicken AlexaFluor 488 (1:1,000 dilution)	Jackson ImmunoResearch Laboratories, #703-545-155	RRID: AB_2340375	
Antibody	Donkey anti-rabbit AlexaFluor 546 (1:1,000 dilution)	Invitrogen; #A-10040	RRID: AB_2534016	
Antibody	Donkey anti-rat AlexaFluor 647 (1:1,000 dilution)	Abcam; #ab150155	RRID: AB_2813835	

Hierarchical Clustering. To resolve whether v-PNs that express distinct 5-HT receptors innervate distinct glomeruli, we hierarchically clustered[111] individual 5-HT receptor-expressing v-PNs by the complement of AL glomeruli each v-PN innervates. Briefly, individual 5-HT receptor-expressing v-PNs were hierarchically clustered using Ward's method ("ward.D2") and Euclidean distance using the "dist", "hclust", and "as.dendrogram" functions of the base-R *stats* package. The optimal number of k-clusters for this dendrogram was computed using two distinct methods: (1) calculating the maximal average silhouette width using the "find_k" function of the *dendextend* package; and (2) calculating the gap statistic using the "NbClust" function of the *NbClust* package. Both methods identified that two k-clusters were optimal for the underlying data being hierarchically clustered.

Connectomic analysis

Connectomic analyses in Fig. 7 were performed using the Hemibrain v.1.2.1 dataset[67] accessed via neuPrintExplorer (https://neuprint.janelia.org/). Within this dataset, nine v-PNs were identified as candidates for the v-PNs expressed by the R24H08 and R86G06 LexA driver lines. These were identified based on their glomerular innervation and their projection patterns within the lateral horn, and the number of v-PNs with these characteristics were consistent with the number of cells observed within each driver line (5 for R24H08-LexA and 4 for R86G06-LexA). To determine the postsynaptic partners of each v-PN, the downstream partners were queried for each individual v-PN, and an arbitrary threshold of three synapses was set for inclusion. Postsynaptic targets that were an "orphan" or not ascribed to a cell class within neuPrint were also excluded from analysis. To determine the degree to which v-PNs from R24H08 and R86G06 converged upon the same postsynaptic partners, the "common connectivity" query was used for all nine v-PNs simultaneously. An arbitrary threshold of 3 synapses was set for inclusion and the resultant connectivity table was exported to generate graph plots using CytoScape v3.9.1. The body IDs for the 5 v-PNs similar to those in R24H08, the 4 v-PNs in R86G06 and all shared partners are listed in Table 3. The correlation matrix was generated by querying the downstream connectivity of the R24H08-like and R86G06-like v-PNs in the LH with the "neuprint_connection_table" function of the *neuprintr* package (https://natverse.org/neuprintr/), then computing the Pearson pairwise correlation of columns of the connectivity matrix with the.corr method of the pandas package, where each column contains the downstream connectivity of each individual v-PN. Values for Fig. 1Sf were calculated by the number of synapses onto each 3rd-order olfactory neuron from v-PNs or lv-PNs divided by the total number of postsynapses from v-PNs or lv-PNs. This value was multiplied by, for each 3rd-order olfactory neuron and for each neuropil, the number of postsynaptic sites from 3rd-order olfactory neurons in each neuropil, divided by the total number of postsynaptic sites of each 3rd-order olfactory neuron. The neuropil value plotted is the sum of this value for every 3rd-order olfactory neuron for the corresponding neuropil and its mirror, normalized to 1 being the neuropil with the maximum. Values were generated from fafbseg-py and braincircuits (https://braincircuits.io) in FlyWire FAFB[25,26,112,113].

Pharmacology

Pharmacological agents and their concentrations used in this study. 5-HT (10^{-5}M Serotonin hydrochloride, TCI Chemicals, CAS:153-98-0) was made fresh every day before the start of experiments and the aliquot was shielded from light, the 5-HT receptor antagonist (10^{-5}M Methiothepine mesylate salt, also called metitipine, Sigma, CAS:74611-28-2), 5-HT1A receptor antagonist (10^{-5}M WAY-100635 maleate, Abcam, CAS:634908-75-1), 5-HT1A receptor agonist (10^{-5}M Ipsapirone, Rndsystems, CAS:95847-70-4), 5-HT7 receptor antagonist (10^{-5}M Sb 258719, Tocris, CAS:1217674-10-6), 5-HT7 Receptor agonist (10^{-5}M AS-19, Tocris, CAS:1000578-26-6). The stock solutions of these drugs were diluted in extracellular physiological saline which contained: 103 mM NaCl, 3 mM KCl, 5 mM TES, 8 mM Trehalose, 10 mM Glucose, 26 mM $NaHCO_3$, 1 mM NaH_2PO_4, 1.5 mM $CaCl_2$, 4 mM $MgCl_2$, pH was then adjusted to 7.2 with NaOH.

Fly preparation for in vivo Ca^{2+} imaging and odor delivery. All in vivo Ca^{2+} imaging experiments were performed using a custom-built (Scientifica, Clarksburg, USA) 2-photon microscope system and Mai Tai HP Ti Sapphire laser (Spectra-Physics, Milpitas, CA). Preparations were visualized using a Retiga R6 Microscope Camera (QImaging, Surrey, Canada), data acquired with a gallium arsinide phosphide (GaAsP) photomultiplier tube detector and ScanImage acquisition software (v.5.5, Vidrio Technologies). All recordings were taken at a frame rate of 3.4 Hz. Both male and female flies were used in experiments. For fly preparation for recordings, flies were anesthetized on ice and then placed on the recording dish containing a square aluminum foil sheet (10 mm x 12 mm) in the center of a plastic dish with an imaging window (~ 1 mm x 1 mm) sized to affix a fly. Once the fly was securely positioned, it was then permanently fixed using an LED-UV plastic welder kit (BONDIC, SK8024, NY). Once the fly was glued in place with the head fixed so that the antennae remained dry during saline application, then a small incision was made using 26-gauge needles (BD PrecisionGlide Needle, 305110-26 g, NJ) and covering tissue was then removed in order to expose the dorsal side of the brain. The R86G06 driver line includes OSNs projecting to the DC4 glomerulus, so we only visualized the LH axon terminals for Ca^{2+} imaging of odor-evoked responses.

The recording chamber had a capacity to hold ~3 ml of saline solution and was filled with approximately this amount during the experiment. After the bath application of the drug, there was an 8-minute waiting period before resuming the Ca^{2+} imaging. Odorants used in experiments: 1-Hexanol (Sigma Aldrich, cat. no.471402), 1-octen-3-ol (Sigma Aldrich, cat. no. O5284), Benzaldehyde (Sigma Aldrich, cat. no. B1334), ACV (Heinz), Farnesol (Sigma Aldrich, cat. no. F203), Orange Peel, Acetic Acid (Sigma Aldrich, cat. no. A6283), Acetophenine (Sigma Aldrich, cat. no. A10701), 1:100 dilution was used for all odors and

Table 2 | Genotype of flies in each figure

Figure	Genotype	Purpose
Fig. 1a	w*,10XUAS-IVS-mCD8::RFP,13XLexAop2-mCD8::GFP;;5-HT2B-T2A-GAL4^{MI05208}/TI{2A-lexA::GAD}5-HT2B	Intersection of v-PNs included in the 5-HT2B T2A Gal4 and 5-HT2B T2A LexA driver lines
Fig. 1b	w*,10XUAS-IVS-mCD8::RFP,13XLexAop2-mCD8::GFP;5-HT1A-T2A-GAL4^{MI04464};TI{2A-lexA::GAD}5-HT2B	Intersection of v-PNs included in the 5-HT1A T2A Gal4 and 5-HT2B T2A LexA driver lines
Fig. 1c	w*,10XUAS-IVS-mCD8::RFP,13XLexAop2-mCD8::GFP;;5-HT7-GAL4^{MI00215}/TI{2A-lexA::GAD}5-HT2B	Intersection of v-PNs included in the 5-HT7 T2A Gal4 and 5-HT2B T2A LexA driver lines
S. Fig. 1b	w*,10XUAS-IVS-mCD8::RFP,13XLexAop2-mCD8::GFP;;Mi{Trojan-lexA:QFAD.2}Gad1[MI09277-TlexA:QFAD.2]/+	Depiction of fascicle formed by primary neurites of GABAergic v-PNs as they enter the AL
S. Fig. 1c	w*,10XUAS-IVS-mCD8::RFP,13XLexAop2-mCD8::GFP;;Mi{Trojan-lexA:QFAD.0}ChAT[MI04508-TlexA:QFAD.0]/TM3	Depiction of fascicle formed by primary neurites of cholinergic lv-PNs as they enter the AL
S. Fig. 1g,l	w*,10XUAS-IVS-mCD8::RFP,13XLexAop2-mCD8::GFP;5-HT1A-T2A-GAL4^{MI04464};TI{2A-lexA::GAD}5-HT2B	Intersection of v-PNs included in the 5-HT1A T2A Gal4 and 5-HT2B T2A LexA driver lines
S. Fig. 1h, m	w*,10XUAS-IVS-mCD8::RFP,13XLexAop2-mCD8::GFP;5-HT1B-T2A-GAL4^{MI05213};TI{2A-lexA::GAD}5-HT2B	Intersection of v-PNs included in the 5-HT1B T2A Gal4 and 5-HT2B T2A LexA driver lines
S. Fig. 1i, n	w*;lexAop RFP-UAS GFP; 5-HT2A-T2A-GAL4^{MI00459}/TI{2A-lexA::GAD}5-HT2B	Intersection of v-PNs included in the 5-HT2A T2A Gal4 and 5-HT2B T2A LexA driver lines
S. Fig. 1j, o	w*,10XUAS-IVS-mCD8::RFP,13XLexAop2-mCD8::GFP;;5-HT2B-T2A-GAL4^{MI05208}/TI{2A-lexA::GAD}5-HT2B	Intersection of v-PNs included in the 5-HT2B T2A Gal4 and 5-HT2B T2A LexA driver lines
S. Fig. 1k, p	w*,10XUAS-IVS-mCD8::RFP,13XLexAop2-mCD8::GFP;;5-HT7-GAL4^{MI00215}/TI{2A-lexA::GAD}5-HT2B	Intersection of v-PNs included in the 5-HT7 T2A Gal4 and 5-HT2B T2A LexA driver lines
S. Fig. 1q, u	w*,10XUAS-IVS-mCD8::RFP,13XLexAop2-mCD8::GFP;5-HT1A-T2A-GAL4^{MI04464};TI{2A-lexA::GAD}5-HT7	Intersection of v-PNs included in the 5-HT1A T2A Gal4 and 5-HT7 T2A LexA driver lines
S. Fig. 1r, v	w*,10XUAS-IVS-mCD8::RFP,13XLexAop2-mCD8::GFP;5-HT1B-T2A-GAL4^{MI05213};TI{2A-lexA::GAD}5-HT7	Intersection of v-PNs included in the 5-HT1B T2A Gal4 and 5-HT7 T2A LexA driver lines
S. Fig. 1s, w	w*;lexAop RFP-UAS GFP; 5-HT2A-T2A-GAL4^{MI00459}/TI{2A-lexA::GAD}5-HT7	Intersection of v-PNs included in the 5-HT2A T2A Gal4 and 5-HT7 T2A LexA driver lines
S. Fig. 1t,x	w*,10XUAS-IVS-mCD8::RFP,13XLexAop2-mCD8::GFP;;5-HT7-GAL4^{MI00215}/TI{2A-lexA::GAD}5-HT7	Intersection of v-PNs included in the 5-HT7 T2A Gal4 and 5-HT7 T2A LexA driver lines
S. Fig. 2a	hs-FLPG5.PEST/yw;5-HT1B-T2A-GAL4^{MI05213};10xUAS(FRT.stop)myr::smGdP-HA}VK00005,10xUAS(FRT.stop)myr::smGdP-V5-THS-,10xUAS(FRT.stop)myr::smGdP-FLAG	Example AL and LH of clones from MCFO of 5-HT1B expressing v-PNs
S. Fig. 2b	hs-FLPG5.PEST/yw;;10xUAS(FRT.stop)myr::smGdP-HA}VK00005,10xUAS(FRT.stop)myr::smGdP-V5-THS-,10xUAS(FRT.stop)myr::smGdP-FLAG/5-HT2A-T2A-GAL4^{MI00459}	Example AL and LH of clones from MCFO of 5-HT2A expressing v-PNs
S. Fig. 2c	hs-FLPG5.PEST/yw;;10xUAS(FRT.stop)myr::smGdP-HA}VK00005,10xUAS(FRT.stop)myr::smGdP-V5-THS-,10xUAS(FRT.stop)myr::smGdP-FLAG/5-HT7-GAL4^{MI00215}	Example AL and LH of clones from MCFO of 5-HT7 expressing v-PNs
Fig. 3a, b	w*/yw;UAS-C3PA-GFP/5-HT1A-T2A-GAL4^{MI04464}; + /TM6B	Projection patterns observed after photoactivation of v-PNs expressing the 5-HT1A receptor
Fig. 3c	w*/yw;UAS-C3PA-GFP/5-HT1B-T2A-GAL4^{MI05213}; + /TM6B	Projection patterns observed after photoactivation of v-PNs expressing the 5-HT1B receptor
Fig. 3d	w*/yw;UAS-C3PA-GFP/ + ;5-HT7-GAL4^{MI00215}/TM6B	Projection patterns observed after photoactivation of v-PNs expressing the 5-HT7 receptor
Fig. 4a	w*;;R24H08-GAL4/40XUAS-IVS-mCD8::GFP	Morphology of R24H08 v-PNs in the AL and LH
Fig. 4b	w*;;R86G06-GAL4/40XUAS-IVS-mCD8::GFP	Morphology of R86G06 v-PNs in the AL and LH
Fig. 4e	w*,10XUAS-IVS-mCD8::RFP,13XLexAop2-mCD8::GFP;R24H08-LexA/5-HT1A-T2A-GAL4^{MI04464}	Intersection of v-PNs included in the 5-HT1A T2A Gal4 and R24H08-LexA
Fig. 4f	w*,10XUAS-IVS-mCD8::RFP,13XLexAop2-mCD8::GFP;R24H08-LexA/5-HT1B-T2A-GAL4^{MI05213}	Intersection of v-PNs included in the 5-HT1B T2A Gal4 and R24H08-LexA
Fig. 4g	w*,10XUAS-IVS-mCD8::RFP,13XLexAop2-mCD8::GFP;R86G06-LexA;5-HT7-T2A-GAL4^{MI00215}	Intersection of v-PNs included in the 5-HT7 T2A Gal4 and R86G06-LexA
Fig. 4i, j	w*;10XUAS-IVS-mCD8::GFP;R24H08-GAL4	R24H08-Gal4 stably expressing GFP for HCR labeling against the 5-HT1A and 5-HT1B receptors
Fig. 4k	w*;10XUAS-IVS-mCD8::GFP;R86G06-GAL4	R86G06-Gal4 stably expressing GFP for HCR labeling against the 5-HT7 receptors
S. Fig. 3a, b	w*;R24H08-AD;VT046303-DBD/40XUAS-IVS-mCD8::GFP	Validation of splitGal4 for v-PNs in R24H08
S. Fig. 3c	w*;R24H08-AD/lexAop RFP-UAS GFP;VT046303-DBD/GAD1-Trojan-LexA	Verifying R24H08 v-PNs express GAD1
S. Fig. 3d	w*;lexAop RFP-UAS GFP; R86G06-LexA/GAD1-Trojan-LexA	Verifying R86G06 v-PNs express GAD1
S. Fig. 3e, f	w*;R24H08-LexA/lexAop RFP-UAS GFP;Mz699-Gal4	Verifying R24H08 v-PNs are included in Mz699 v-PNs
S. Fig. 3g, h	w*;R86G06-LexA/lexAop RFP-UAS GFP;Mz699-Gal4	Verifying R86G06 v-PNs are included in Mz699 v-PNs
S. Fig. 3i	w*,10XUAS-IVS-mCD8::RFP,13XLexAop2-mCD8::GFP;R24H08-LexA/5-HT1A-T2A-GAL4^{MI04464}	Intersection of v-PNs included in the 5-HT1A T2A Gal4 and R24H08-LexA
S. Fig. 3j	w*,10XUAS-IVS-mCD8::RFP,13XLexAop2-mCD8::GFP;R24H08-LexA/5-HT1B-T2A-GAL4^{MI05213}	Intersection of v-PNs included in the 5-HT1B T2A Gal4 and R24H08-LexA

Table 2 (continued) | Genotype of flies in each figure

Figure	Genotype	Purpose
S. Fig. 3k	w*;R24H08-LexA/lexAop RFP-UAS GFP;5-HT2A-T2A-GAL4^{MI00459}	Intersection of v-PNs included in the 5-HT2A T2A Gal4 and R24H08-LexA
S. Fig. 3l	w*,10XUAS-IVS-mCD8::RFP,13XLexAop2-mCD8::GFP;R24H08-LexA/5-HT2B-T2A-GAL4^{MI05208}	Intersection of v-PNs included in the 5-HT2B T2A Gal4 and R24H08-LexA
S. Fig. 3m	w*,10XUAS-IVS-mCD8::RFP,13XLexAop2-mCD8::GFP;R24H08-LexA;5-HT7-T2A-GAL4^{MI00215}	Intersection of v-PNs included in the 5-HT7 T2A Gal4 and R24H08-LexA
S. Fig. 3n	w*,10XUAS-IVS-mCD8::RFP,13XLexAop2-mCD8::GFP;R86G06-LexA/5-HT1A-T2A-GAL4^{MI04464};	Intersection of v-PNs included in the 5-HT1A T2A Gal4 and R86G06-LexA
S. Fig. 3o	w*,10XUAS-IVS-mCD8::RFP,13XLexAop2-mCD8::GFP;R86G06-LexA/5-HT1B-T2A-GAL4^{MI05213};	Intersection of v-PNs included in the 5-HT1B T2A Gal4 and R86G06-LexA
S. Fig. 3p	w*;R86G06-LexA/lexAop RFP-UAS GFP;5-HT2A-T2A-GAL4^{MI00459}	Intersection of v-PNs included in the 5-HT2A T2A Gal4 and R86G06-LexA
S. Fig. 3q	w*,10XUAS-IVS-mCD8::RFP,13XLexAop2-mCD8::GFP;R86G06-LexA/5-HT2B-T2A-GAL4^{MI05208}	Intersection of v-PNs included in the 5-HT2B T2A Gal4 and R86G06-LexA
S. Fig. 3r	w*,10XUAS-IVS-mCD8::RFP,13XLexAop2-mCD8::GFP;R86G06-LexA;5-HT7-T2A-GAL4^{MI00215}	Intersection of v-PNs included in the 5-HT7 T2A Gal4 and R86G06-LexA
Fig. 5a, b	w*;;R86G06-GAL4/20XUAS-IVS-jGCaMP7f w*;R24H08-AD/ + ;VT046303-DBD/20XUAS-IVS-jGCaMP7f	Ca2+ imaging of odor responses from R24H08 and R86G06 v-PNs
Fig. 5c, d	w*;R86G06-LexA/UAS-CsChr;R60F02-Gal4/lexAop-jGCaMP7f	Ca^{2+} imaging of odor responses from R86G06 v-PNs with or without preceding optogenetic activation of the CSDns via R60F02.
Fig. 5e, f	w*;R24H08-LexA/UAS-CsChr;R60F02-Gal4/lexAop-jGCaMP7f	Ca^{2+} imaging of odor responses from R24H08 v-PNs with or without preceding optogenetic activation of the CSDns via R60F02.
S. Fig. 4a, b	w*;+/UAS-CsChr;R60F02-Gal4/UAS-jGCaMP7f	Ca^{2+} imaging of optogenetically stimulated activation of CSDns
S. Fig. 4c, d	w*;R86G06-LexA/UAS-CsChr;R60F02-Gal4/lexAop-jGCaMP7f	Ca^{2+} imaging of R86G06 v-PNs with optogenetic activation of CSDns
S. Fig. 4e, f	w*;R24H08-LexA/UAS-CsChr;R60F02-Gal4/lexAop-jGCaMP7f	Ca^{2+} imaging of R24H08 v-PNs with optogenetic activation of CSDns
Fig. 6a, b	w*;+/20XUAS-IVS-jGCaMP7f;R86G06-Gal4/+	Ca^{2+} imaging of odor responses from R86G06 v-PNs before and after application of Serotonin(5-HT) and AS-19
Fig. 6c	w*;+/20XUAS-IVS-jGCaMP7f;R86G06-GAL4/UAS-5-HT$_7$RNAi	Ca^{2+} imaging of odor responses from R86G06 v-PNs while driving $5HT_7$ receptor RNAi
Fig. 6d, e	w*;R24H08-AD/20XUAS-IVS-jGCaMP7f;VT046303-DBD	Ca^{2+} imaging of odor responses from R24H08 v-PNs before and after application of Serotonin(5-HT) and Ipsapirone
Fig. 6f	w*;R24H08-AD/20XUAS-IVS-jGCaMP7f;VT046303-DBD/UAS-5-HT$_{1a}$RNAi	Ca^{2+} imaging of odor responses from R24H08 v-PNs while driving $5HT_{1A}$ receptor RNAi
S. Fig. 5a, b	w*;+/20XUAS-IVS-jGCaMP7f;R86G06-GAL4/+	Ca^{2+} imaging of odor responses from R86G06 v-PNs before and after application of Metitipine and SB-269970
S. Fig. 5c–f	w*;R24H08-AD/20XUAS-IVS-jGCaMP7f;VT046303-DBD/+	Ca^{2+} imaging of odor responses from R24H08 v-PNs before and after application of Serotonin (5-HT), Ipsapirone, Metitipine, WAY100635
S. Fig. 5g	w*;20XUAS-IVS-jGCaMP7f/+;R86G06-GAL4/+ w*;R24H08-AD/20XUAS-IVS-jGCaMP7;VT046303-DBD/+	Baseline Ca^{2+} change of R24H08 and R86G06 v-PNs and bath application of Ipsapirone and AS-19
S. Fig. 5h, i	w*,10XUAS-IVS-mCD8::RFP,13XLexAop2-mCD8::GFP;R24H08-LexA/+;R60F02-Gal4/+	Depiction of overlap in projection of R24H08 v-PNs and the CSDns in the AL and LH
S. Fig. 5j	w*,10XUAS-IVS-mCD8::RFP,13XLexAop2-mCD8::GFP;R86G06-LexA/+;R60F02-Gal4/+	Depiction of overlap in projection of R86G06 v-PNs and the CSDns in the LH
Fig. 7a	w*;lexAop-rCD2::RFP-p10.UAS-mCD8::GFP-p10/R24H08-LexA;R86G06-GAL4	Comparing morphology of R24H08 and R86G06 v-PNs

diluted in mineral oil (Sigma Aldrich, cat. no. M5904). Odors were delivered as previously[114]. Briefly, odorant dilutions were pipetted onto pieces of Whatman filter paper in 5cc glass syringes with 20-gauge needles inserted through a rubber septum (Thermogreen LB-2 Septa, 20633, Bellefonte, PA) into a common air stream directed at the antennae. Common and odor air streams originated from compressed air that was first carbon filtered, then re-humidified before being split to the constant airflow line (2.5 L/min regulated using a Dwyer VFA-25-BV flowmeter) and the airflow (.8 L/min regulator using a Dwyer VFA-23-BV flowmeter) delivered to a solenoid (Parker, 001-0028-900, Hollis, NH) that could switch between an empty cartridge and an odor cartridge. Custom MatLab script (Matlab version 2018b, provided by Kaleb Hatch) was used to send a 5 V TTL pulse to a 50 W power source (CUI Inc, 102-3295-ND, Tualatin, OR) to actuate the solenoid. Constant airflow was directed to the antennae via a central glass tube with two ports holding rubber septa into which the empty cartridge and odor cartridge could be inserted to introduce a second airstream at a 45° angle. Odorants were delivered by activating the solenoid to switch the second airflow from the empty cartridge to the odor cartridge for 2-3 times, depending on the experimental protocol, for 1s.

For optogenetic activation of CSDn neurons, a red LED (FT800EMT-Custom Fiber Patch Cable, 2.5 mm End, Thorlabs) controlled by a T-Cube LED current controller (Thorlabs) delivered light intensity of 5-8 mW/mm² from beneath the recording dish. A notch filter (Edmund Optic, 14770 Filter Ultrathin Notch OD6 633 nm, 25 mmD) was inserted into the light path to help mitigate the red-light

Table 3 | Hemibrain Body IDs for all neurons in the connectomic analysis

Neuron	Body ID	Descriptor
R24H08-like v-PN	5813077810	v-PN resembling R24H08-Gal4 v-PNs
R24H08-like v-PN	1857143769	v-PN resembling R24H08-Gal4 v-PNs
R24H08-like v-PN	948834414	v-PN resembling R24H08-Gal4 v-PNs
R24H08-like v-PN	1889883818	v-PN resembling R24H08-Gal4 v-PNs
R24H08-like v-PN	1415825344	v-PN resembling R24H08-Gal4 v-PNs
R86G06-like v-PN	791298858	v-PN resembling R86G06-Gal4 v-PNs
R86G06-like v-PN	760264077	v-PN resembling R86G06-Gal4 v-PNs
R86G06-like v-PN	729219639	v-PN resembling R86G06-Gal4 v-PNs
R86G06-like v-PN	698526273	v-PN resembling R86G06-Gal4 v-PNs
LHN downstream of R24H08-like v-PNs	855384597	LHCENT
LHN downstream of R24H08-like v-PNs	913754682	LHON
LHN downstream of R24H08-like v-PNs	1260582361	LHON
LHN downstream of R24H08-like v-PNs	1006146837	LHCENT
LHN downstream of R24H08-like v-PNs	759582415	LHLN
LHN downstream of R24H08-like v-PNs	821612285	LHON
LHN downstream of R24H08-like v-PNs	822687493	LHLN
LHN downstream of R24H08-like v-PNs	819895218	LHON
LHN downstream of R24H08-like v-PNs	852302293	LHON
LHN downstream of R24H08-like v-PNs	730562993	LHON
LHN downstream of R86G06-like v-PNs	698185483	LHLN
LHN downstream of R86G06-like v-PNs	546123239	LHON
LHN downstream of R86G06-like v-PNs	698180927	LHLN
LHN downstream of R86G06-like v-PNs	574377562	LHON
LHN downstream of R86G06-like v-PNs	882685590	LHLN
LHN downstream of R86G06-like v-PNs	510317265	LHLN
LHN downstream of R86G06-like v-PNs	417186612	LHLN
LHN downstream of R86G06-like v-PNs	421641859	LHON
LHN downstream of R86G06-like v-PNs	666136034	LHON
LHN downstream of R86G06-like v-PNs	5813011024	LHON
LHN downstream of R86G06-like v-PNs	510934715	LHLN
LHN downstream of R86G06-like v-PNs	758178605	LHLN

intensity and protect the photomultiplier tube. In experiments involving only CSDn stimulation, neurons were stimulated optogenetically for 1 second, repeated 3 times within a 60-second recording. Frames during the red-light stimulation were removed due to interference with the two-photon sensor. In experiments co-activating CSDn and v-PNs, the R24H08 and R86G06 v-PN populations were stimulated with benzaldehyde (3 ×1-second pulses). Prior to the second benzaldehyde pulse, CSDn neurons were optogenetically activated for 1 second, followed by a 15 ms delay before the odor pulse. Frames during optogenetic activation were removed in this paradigm as well.

Raw imaging data was then imported into FIJI, and then ROIs were drawn. Extracted ROI fluorescence signal data was then processed using a custom Matlab Script which normalized to baseline fluorescence signals (F, fluorescence averaged across 3 seconds before the first odor stimulation) and data was visualized as percent change in fluorescence from average values (ΔF/F), script then produced representation of percent change in fluorescence as a Heatmap (Matlab version 2018b, script provided by Keshav L. Ramachandra) or average ΔF/F odor responses were then processed in graphpad for statistical analysis.

GFP-photoactivation

Photoactivatable GFP experiments were completed using a 2-photon vivoscope with Mai Tai HP Ti Sapphire laser and a stimulation protocol adjusted from prior descriptions[115]. Stimulation was produced using ScanImage acquisition software and timing was controlled with a custom script written in Daq EventTimer[116]. Flies were prepared by severing the fly head, removing the antennae and proboscis under physiological saline (see above), then peeling the clypeus to vertex away to expose the ALs. Tungsten wires were used to stabilize the head. Cells were located using a wavelength of 940 nm, outside of the photoactivatable range for GFP. Cells were stimulated with 9-11 mW/cm^2 at 710 nm with power delivery controlled digitally through a Pockel cell (Model: 350-80-02LA, Conoptics, Danbury, CT). Stimulation was delivered in a 40 μM^2 scanning window with 2μs pixel dwell time. Cells were stimulated by acquiring 100 frames, with each frame separated by 5.6 seconds. This acquisition period was repeated 3 times, with each series followed by 45 minutes. After the third 45-minute break, each brain was individually dissected and incubated in 4% paraformaldehyde on ice for 25 minutes. Brains were each processed as described above for N-Cadherin immunolabeling, and only endogenous GFP fluorescence was used rather than GFP immunolabeling. Confocal scans were collected as described above and.oib files obtained from confocal imaging were analyzed using Fiji ImageJ. Using the NCAD channel as a reference, the volume of the lateral horn was cropped away from the GFP channel for every slice in the stack. This was done to remove influence from natively activated paGFP from surrounding cell bodies. Using a custom-written Java ImageJ plugin (https://github.com/JohnHageter/Binned_Intensity/), a polygonal ROI was drawn around the lateral horn on a max projection of the image stack. The bounding box of the drawn ROI was segmented into a 10 ×10

bin grid. We measured the average intensity from each channel within the bins and normalized this to the bin with the maximum average intensity, whose center was within the previously drawn ROI. Segmented bins whose centers were located outside of the lateral horn were removed from further analysis. Statistical analysis for photoactivatable experiments was carried out in R (R Core Team). An independence test was generated for each receptor and bin position. Post-Hoc comparisons were TukeyHSD and found using the "glht" function for the "multicomp" package.

Statistical analyses

The number of animals used in each experiment was between 8 and 12 (number of animals and trials are stated in figure legends). Statistical analysis was carried out using GraphPad Prism software (GraphPad Prism version 8.0, 2018). Shapiro-Wilk normality tests were used to determine if data was normally distributed. Paired sample T-tests were performed in all Ca^{2+} datasets and passed. For the pharmacological Ca^{2+} imaging data, paired sample T-tests were performed for normally distributed data to compare responses before and after drug application. For the optogenetic experiments, in R24 optogenetic experiments where data was not normally distributed, Friedman tests were used followed by Dunn's post-hoc tests for multiple comparisons. In R86 optogenetic experiments where data were normally distributed, repeated measures ANOVAs were performed, followed by Tukey's HSD post-hoc tests. For all dot plots the center line represents the mean and whiskers represent 1 standard deviation. No outliers were removed from our analyses.

Materials and reagents availability

All *Drosophila* stocks in this paper were derived from stocks available from the Bloomington stock center, or as gifts and all chemical reagents are commercially available (see Table 1).

Reporting summary

Further information on research design is available in the Nature Portfolio Reporting Summary linked to this article.

Data availability

All data supporting the findings of this study are available at Identifier: https://doi.org/10.17605/OSF.IO/ZYSVP.

Code availability

Custom FIJI plugin for polygonal ROI analysis in PA-GFP experiments: https://github.com/JohnHageter/Binned_Intensity/.

References

1. Root, C. M. et al. A presynaptic gain control mechanism fine-tunes olfactory behavior. *Neuron* **59**, 311–321 (2008).
2. Olsen, S. R. & Wilson, R. I. Lateral presynaptic inhibition mediates gain control in an olfactory circuit. *Nature* **452**, 956–960 (2008).
3. Olsen, S. R., Bhandawat, V. & Wilson, R. I. Divisive normalization in olfactory population codes. *Neuron* **66**, 287–299 (2010).
4. Wang, J. W. Presynaptic modulation of early olfactory processing in Drosophila. *Dev. Neurobiol.* **72**, 87–99 (2012).
5. Pírez, N. & Wachowiak, M. In vivo modulation of sensory input to the olfactory bulb by tonic and activity-dependent presynaptic inhibition of receptor neurons. *J. Neurosci.* **28**, 6360–6371 (2008).
6. Wachowiak, M. & Cohen, L. B. Presynaptic inhibition of primary olfactory afferents mediated by different mechanisms in lobster and turtle. *J. Neurosci.* **19**, 8808–8817 (1999).
7. Wachowiak, M. et al. Inhibition [corrected] of olfactory receptor neuron input to olfactory bulb glomeruli mediated by suppression of presynaptic calcium influx. *J. Neurophysiol.* **94**, 2700–2712 (2005).
8. Kim, S. M., Su, C.-Y. & Wang, J. W. Neuromodulation of innate behaviors in drosophila. *Annu. Rev. Neurosci.* **40**, 327–348 (2017).
9. Alcedo, J. & Prahlad, V. Neuromodulators: an essential part of survival. *J. Neurogenet.* **34**, 475–481 (2020).
10. Flavell, S. W., Raizen, D. M. & You, Y.-J. Behavioral States. *Genetics* **216**, 315–332 (2020).
11. Brunert, D., Tsuno, Y., Rothermel, M., Shipley, M. T. & Wachowiak, M. Cell-Type-Specific Modulation of Sensory Responses in Olfactory Bulb Circuits by Serotonergic Projections from the Raphe Nuclei. *J. Neurosci.* **36**, 6820–6835 (2016).
12. Suzuki, Y., Schenk, J. E., Tan, H. & Gaudry, Q. A population of interneurons signals changes in the basal concentration of serotonin and mediates gain control in the drosophila antennal lobe. *Curr. Biol.* **30**, 1110–1118.e4 (2020).
13. Kaneko, T. et al. Serotonergic modulation enables pathway-specific plasticity in a developing sensory circuit in drosophila. *Neuron* **95**, 722 (2017).
14. Sizemore, T. R., Jonaitis, J. & Dacks, A. M. Heterogeneous receptor expression underlies non-uniform peptidergic modulation of olfaction in Drosophila. *Nat. Commun.* **14**, 5280 (2023).
15. Ignell, R. et al. Presynaptic peptidergic modulation of olfactory receptor neurons in Drosophila. *Proc. Natl Acad. Sci. USA* **106**, 13070–13075 (2009).
16. Ko, K. I. et al. Starvation promotes concerted modulation of appetitive olfactory behavior via parallel neuromodulatory circuits. *eLife*. **4**, https://doi.org/10.7554/eLife.08298 (2015).
17. Sizemore, T. R. & Dacks, A. M. Serotonergic Modulation Differentially Targets Distinct Network Elements within the Antennal Lobe of Drosophila melanogaster. *Sci. Rep.* **6**, 37119 (2016).
18. Gasque, G., Conway, S., Huang, J., Rao, Y. & Vosshall, L. B. Small molecule drug screening in Drosophila identifies the 5HT2A receptor as a feeding modulation target. *Sci. Rep.* **3**, srep02120 (2013).
19. Nichols, D. E. & Nichols, C. D. Serotonin receptors. *Chem. Rev.* **108**, 1614–1641 (2008).
20. Tierney, A. J. Invertebrate serotonin receptors: a molecular perspective on classification and pharmacology. *J. Exp. Biol.* **221**, https://doi.org/10.1242/jeb.184838 (2018).
21. Lai, S.-L., Awasaki, T., Ito, K. & Lee, T. Clonal analysis of Drosophila antennal lobe neurons: diverse neuronal architectures in the lateral neuroblast lineage. *Development* **135**, 2883–2893 (2008).
22. Strutz, A. et al. Decoding odor quality and intensity in the Drosophila brain. *eLife* **3**, e04147 (2014).
23. Bates, A. S. et al. Complete connectomic reconstruction of olfactory projection neurons in the fly brain. *Curr. Biol.* **30**, 3183–3199.e6 (2020).
24. Schlegel, P. et al. Information flow, cell types and stereotypy in a full olfactory connectome. *eLife 10*. (2021).
25. Dorkenwald, S. et al. FlyWire: online community for whole-brain connectomics. *Nat. Methods* **19**, 119–128 (2022).
26. Zheng, Z. et al. A Complete Electron Microscopy Volume of the Brain of Adult Drosophila melanogaster. *Cell* **174**, 730–743.e22 (2018).
27. Tanaka, N. K., Endo, K. & Ito, K. Organization of antennal lobe-associated neurons in adult Drosophila. *melanogaster brain. J. Comp. Neurol.* **520**, 4067–4130 (2012).
28. Sachse, S. & Beshel, J. The good, the bad, and the hungry: how the central brain codes odor valence to facilitate food approach in Drosophila. *Curr. Opin. Neurobiol.* **40**, 53–58 (2016).
29. Das Chakraborty, S. & Sachse, S. Olfactory processing in the lateral horn of Drosophila. *Cell Tissue Res.* **383**, 113–123 (2021).
30. Schultzhaus, J. N., Saleem, S., Iftikhar, H. & Carney, G. E. The role of the Drosophila lateral horn in olfactory information processing and behavioral response. *J. Insect Physiol.* **98**, 29–37 (2017).
31. Parnas, M., Lin, A. C., Huetteroth, W. & Miesenböck, G. Odor discrimination in Drosophila: from neural population codes to behavior. *Neuron* **79**, 932–944 (2013).

32. Liang, L. et al. GABAergic projection neurons route selective olfactory inputs to specific higher-order neurons. *Neuron* **79**, 917–931 (2013).
33. Jeanne, J. M., Fişek, M. & Wilson, R. I. The organization of projections from olfactory glomeruli onto higher-order neurons. *Neuron* **98**, 1198–1213.e6 (2018).
34. Wang, K. et al. Parallel pathways convey olfactory information with opposite polarities in Drosophila. *Proc. Natl Acad. Sci. USA* **111**, 3164–3169 (2014).
35. Fişek, M. & Wilson, R. I. Stereotyped connectivity and computations in higher-order olfactory neurons. *Nat. Neurosci.* **17**, 280–288 (2014).
36. Semelidou, O., Acevedo, S. F., & Skoulakis, E. M. Temporally specific engagement of distinct neuronal circuits regulating olfactory habituation in Drosophila. *eLife*. **7**, https://doi.org/10.7554/eLife.39569 (2018).
37. Gnerer, J. P., Venken, K. J. T. & Dierick, H. A. Gene-specific cell labeling using MiMIC transposons. *Nucleic Acids Res.* **43**, e56 (2015).
38. Deng, B. et al. Chemoconnectomics: mapping chemical transmission in drosophila. *Neuron* **101**, 876–893.e4 (2019).
39. Nern, A., Pfeiffer, B. D. & Rubin, G. M. Optimized tools for multicolor stochastic labeling reveal diverse stereotyped cell arrangements in the fly visual system. *Proc. Natl Acad. Sci. USA* **112**, E2967–E2976 (2015).
40. Wong, J. Y. H. et al. Octopaminergic neurons have multiple targets in Drosophila larval mushroom body calyx and can modulate behavioral odor discrimination. *Learn. Mem.* **28**, 53–71 (2021).
41. Dolan, M.-J. et al. Communication from Learned to Innate Olfactory Processing Centers Is Required for Memory Retrieval in Drosophila. *Neuron* **100**, 651–668.e8 (2018).
42. Chin, S. G., Maguire, S. E., Huoviala, P., Jefferis, G. S. X. E. & Potter, C. J. Olfactory neurons and brain centers directing oviposition decisions in drosophila. *Cell Rep.* **24**, 1667–1678 (2018).
43. Cachero, S., Ostrovsky, A. D., Yu, J. Y., Dickson, B. J. & Jefferis, G. S. X. E. Sexual dimorphism in the fly brain. *Curr. Biol.* **20**, 1589–1601 (2010).
44. Jefferis, G. S. X. E. et al. Comprehensive maps of Drosophila higher olfactory centers: spatially segregated fruit and pheromone representation. *Cell* **128**, 1187–1203 (2007).
45. Wong, A. M., Wang, J. W. & Axel, R. Spatial representation of the glomerular map in the Drosophila protocerebrum. *Cell* **109**, 229–241 (2002).
46. Choi, K., Kim, W. K., & Hyeon, C. Olfactory responses of Drosophila are encoded in the organization of projection neurons. *eLife*. **11**. https://doi.org/10.7554/eLife.77748 (2022).
47. Datta, S. R. et al. The Drosophila pheromone cVA activates a sexually dimorphic neural circuit. *Nature* **452**, 473–477 (2008).
48. Jenett, A. et al. A GAL4-driver line resource for Drosophila neurobiology. *Cell Rep.* **2**, 991–1001 (2012).
49. Ronderos, D. S., Lin, C.-C., Potter, C. J. & Smith, D. P. Farnesol-detecting olfactory neurons in Drosophila. *J. Neurosci.* **34**, 3959–3968 (2014).
50. Galizia, C. G., Münch, D., Strauch, M., Nissler, A. & Ma, S. Integrating heterogeneous odor response data into a common response model: A DoOR to the complete olfactome. *Chem. Senses* **35**, 551–563 (2010).
51. Knaden, M., Strutz, A., Ahsan, J., Sachse, S. & Hansson, B. S. Spatial representation of odorant valence in an insect brain. *Cell Rep.* **1**, 392–399 (2012).
52. Inamdar, A. A. et al. Fungal-derived semiochemical 1-octen-3-ol disrupts dopamine packaging and causes neurodegeneration. *Proc. Natl Acad. Sci. USA* **110**, 19561–19566 (2013).
53. Kreher, S. A., Mathew, D., Kim, J. & Carlson, J. R. Translation of sensory input into behavioral output via an olfactory system. *Neuron* **59**, 110–124 (2008).
54. Semmelhack, J. L. & Wang, J. W. Select Drosophila glomeruli mediate innate olfactory attraction and aversion. *Nature* **459**, 218–223 (2009).
55. Dweck, H. K. M. et al. Olfactory preference for egg laying on citrus substrates in Drosophila. *Curr. Biol.* **23**, 2472–2480 (2013).
56. Dacks, A. M., Christensen, T. A. & Hildebrand, J. G. Phylogeny of a serotonin-immunoreactive neuron in the primary olfactory center of the insect brain. *J. Comp. Neurol.* **498**, 727–746 (2006).
57. Roy, B. et al. Metamorphosis of an identified serotonergic neuron in the Drosophila olfactory system. *Neural Dev.* **2**, 20 (2007).
58. Singh, A. P. et al. Sensory neuron-derived eph regulates glomerular arbors and modulatory function of a central serotonergic neuron. *PLoS Genet.* **9**, e1003452 (2013).
59. Python, F. & Stocker, R. F. Immunoreactivity against choline acetyltransferase, gamma-aminobutyric acid, histamine, octopamine, and serotonin in the larval chemosensory system of Dosophila. *melanogaster. J. Comp. Neurol.* **453**, 157–167 (2002).
60. Coates, K. E. et al. Identified Serotonergic Modulatory Neurons Have Heterogeneous Synaptic Connectivity within the Olfactory System of Drosophila. *J. Neurosci.* **37**, 7318–7331 (2017).
61. Coates, K. E. et al. The wiring logic of an identified serotonergic neuron that spans sensory networks. *J. Neurosci.* **40**, 6309–6327 (2020).
62. Zhang, X., & Gaudry, Q. Functional integration of a serotonergic neuron in the Drosophila antennal lobe. *eLife*. **5**, https://doi.org/10.7554/eLife.16836 (2016).
63. Vogt, K. et al. Internal state configures olfactory behavior and early sensory processing in Drosophila larvae. *Sci. Adv.* **7**. https://doi.org/10.1126/sciadv.abd6900 (2021).
64. Li, H. et al. Fly Cell Atlas: A single-nucleus transcriptomic atlas of the adult fruit fly. *Science* **375**, eabk2432 (2022).
65. Dacks, A., Green, D., Root, C., Nighorn, A. & Wang, J. Serotonin Modulates Olfactory Processing in the Antennal Lobe of Drosophila. *J. Neurogenet.*, 1–13. (2009).
66. Dacks, A. M., Christensen, T. A. & Hildebrand, J. G. Modulation of olfactory information processing in the antennal lobe of *Manduca sexta* by serotonin. *J. Neurophysiol.* **99**, 2077–2085 (2008).
67. Scheffer, L. K. et al. A connectome and analysis of the adult Drosophila central brain. *eLife*. **9**, https://doi.org/10.7554/eLife.57443 (2020).
68. Dolan, M.-J. et al. Neurogenetic dissection of the Drosophila lateral horn reveals major outputs, diverse behavioural functions, and interactions with the mushroom body. *eLife*. **8**, https://doi.org/10.7554/eLife.43079 (2019).
69. Frechter, S. et al. Functional and anatomical specificity in a higher olfactory centre. *eLife* **8**, 10.7554/eLife.44590 (2019).
70. Sampson, M. M. et al. Serotonergic modulation of visual neurons in Drosophila melanogaster. *PLoS Genet.* **16**, e1009003 (2020).
71. Rister, J. et al. Dissection of the peripheral motion channel in the visual system of Drosophila melanogaster. *Neuron* **56**, 155–170 (2007).
72. Kasture, A. S. et al. Distinct contribution of axonal and somatodendritic serotonin transporters in drosophila olfaction. *Neuropharmacology* **161**, 107564 (2019).
73. He, J., Hommen, F., Lauer, N., Balmert, S. & Scholz, H. Serotonin transporter dependent modulation of food-seeking behavior. *PLoS ONE* **15**, e0227554 (2020).
74. Xu, L. et al. A single pair of serotonergic neurons counteracts serotonergic inhibition of ethanol attraction in drosophila. *PLoS ONE* **11**, e0167518 (2016).
75. Lizbinski, K. M. & Dacks, A. M. Intrinsic and extrinsic neuromodulation of olfactory processing. *Front. Cell. Neurosci.* **11**, 424 (2017).

76. Gaudry, Q. Serotonergic modulation of olfaction in rodents and insects. *Yale J. Biol. Med.* **91**, 23–32 (2018).
77. Sizemore, T. R., Hurley, L. M. & Dacks, A. M. Serotonergic modulation across sensory modalities. *J. Neurophysiol.* **123**, 2406–2425 (2020).
78. Bonanno, S. L. et al. Constitutive and Conditional Epitope Tagging of Endogenous G-Protein-Coupled Receptors in Drosophila. *J. Neurosci.* **44**, https://doi.org/10.1523/JNEUROSCI.2377-23.2024 (2024).
79. Herrick-Davis, K. Functional significance of serotonin receptor dimerization. *Exp. Brain Res.* **230**, 375–386 (2013).
80. Maroteaux, L., Béchade, C. & Roumier, A. Dimers of serotonin receptors: Impact on ligand affinity and signaling. *Biochimie* **161**, 23–33 (2019).
81. Renner, U. et al. Heterodimerization of serotonin receptors 5-HT1A and 5-HT7 differentially regulates receptor signalling and trafficking. *J. Cell Sci.* **125**, 2486–2499 (2012).
82. Taisz, I. et al. Generating parallel representations of position and identity in the olfactory system. *SSRN Journal*. https://doi.org/10.2139/ssrn.4129429 (2022).
83. Das Chakraborty, S., Chang, H., Hansson, B. S. & Sachse, S. Higher-order olfactory neurons in the lateral horn support odor valence and odor identity coding in Drosophila. *eLife*. **11**, https://doi.org/10.7554/eLife.74637 (2022).
84. Campetella, F. et al. Olfactory learning modulates a neural circuit mediating innate odor-guided behavior in Drosophila. *BioRxiv*. https://doi.org/10.1101/2023.09.20.558596 (2023).
85. Mazo, C. et al. Long-range GABAergic projections contribute to cortical feedback control of sensory processing. *Nat. Commun.* **13**, 6879 (2022).
86. Otazu, G. H., Chae, H., Davis, M. B. & Albeanu, D. F. Cortical feedback decorrelates olfactory bulb output in awake mice. *Neuron* **86**, 1461–1477 (2015).
87. Boyd, A. M., Sturgill, J. F., Poo, C. & Isaacson, J. S. Cortical feedback control of olfactory bulb circuits. *Neuron* **76**, 1161–1174 (2012).
88. Marin, E. C., Jefferis, G. S. X. E., Komiyama, T., Zhu, H. & Luo, L. Representation of the glomerular olfactory map in the Drosophila brain. *Cell* **109**, 243–255 (2002).
89. Mansourian, S. & Stensmyr, M. C. The chemical ecology of the fly. *Curr. Opin. Neurobiol.* **34**, 95–102 (2015).
90. Grosjean, Y. et al. An olfactory receptor for food-derived odours promotes male courtship in Drosophila. *Nature* **478**, 236–240 (2011).
91. Stensmyr, M. C. et al. A conserved dedicated olfactory circuit for detecting harmful microbes in Drosophila. *Cell* **151**, 1345–1357 (2012).
92. Zeng, H. & Sanes, J. R. Neuronal cell-type classification: challenges, opportunities and the path forward. *Nat. Rev. Neurosci.* **18**, 530–546 (2017).
93. Cembrowski, M. S. & Spruston, N. Heterogeneity within classical cell types is the rule: lessons from hippocampal pyramidal neurons. *Nat. Rev. Neurosci.* **20**, 193–204 (2019).
94. Okaty, B. W., Commons, K. G. & Dymecki, S. M. Embracing diversity in the 5-HT neuronal system. *Nat. Rev. Neurosci.* **20**, 397–424 (2019).
95. Held, M. et al. Aminergic and peptidergic modulation of insulin-producing cells in Drosophila. *eLife*. **13**, https://doi.org/10.7554/eLife.99548.3 (2025).
96. Chou, Y.-H. et al. Diversity and wiring variability of olfactory local interneurons in the Drosophila antennal lobe. *Nat. Neurosci.* **13**, 439–449 (2010).
97. Hong, E. J. & Wilson, R. I. Simultaneous encoding of odors by channels with diverse sensitivity to inhibition. *Neuron* **85**, 573–589 (2015).
98. Nagel, K. I., Hong, E. J. & Wilson, R. I. Synaptic and circuit mechanisms promoting broadband transmission of olfactory stimulus dynamics. *Nat. Neurosci.* **18**, 56–65 (2015).
99. Seki, Y., Rybak, J., Wicher, D., Sachse, S. & Hansson, B. S. Physiological and morphological characterization of local interneurons in the Drosophila antennal lobe. *J. Neurophysiol.* **104**, 1007–1019 (2010).
100. Reisenman, C. E., Dacks, A. M. & Hildebrand, J. G. Local interneuron diversity in the primary olfactory center of the moth Manduca sexta. *J. Comp. Physiol. A Neuroethol. Sens. Neural Behav. Physiol.* **197**, 653–665 (2011).
101. Lizbinski, K. M., Marsat, G. F. & Dacks, A. M. Transmitter Co-Expression Reveals Key Organizational Principles of Local Interneuron Heterogeneity in the Olfactory System. *BioRxiv*. https://doi.org/10.1101/167403 (2017).
102. Carlsson, M. A., Diesner, M., Schachtner, J. & Nässel, D. R. Multiple neuropeptides in the Drosophila antennal lobe suggest complex modulatory circuits. *J. Comp. Neurol.* **518**, 3359–3380 (2010).
103. Grabe, V. et al. Elucidating the neuronal architecture of olfactory glomeruli in the drosophila antennal lobe. *Cell Rep.* **16**, 3401–3413 (2016).
104. Berck, M. E. et al. The wiring diagram of a glomerular olfactory system. *eLife*. **5**, https://doi.org/10.7554/eLife.14859 (2016).
105. Nath, H. B. Waiting time in the coupon-collector's problem1. *Aust. J. Stat.* **15**, 132–135 (1973).
106. Flajolet, P., Gardy, D. & Thimonier, L. Birthday paradox, coupon collectors, caching algorithms and self-organizing search. *Discret. Appl. Math.* **39**, 207–229 (1992).
107. Diao, F. et al. Plug-and-play genetic access to drosophila cell types using exchangeable exon cassettes. *Cell Rep.* **10**, 1410–1421 (2015).
108. Couto, A., Alenius, M. & Dickson, B. J. Molecular, anatomical, and functional organization of the Drosophila olfactory system. *Curr. Biol.* **15**, 1535–1547 (2005).
109. Laissue, P. P. et al. Three-dimensional reconstruction of the antennal lobe in Drosophila. *melanogaster. J. Comp. Neurol.* **405**, 543–552 (1999).
110. Task, D. et al. Chemoreceptor co-expression in Drosophila melanogaster olfactory neurons. *eLife* **11**, https://doi.org/10.7554/eLife.72599 (2022).
111. Sizemore, T.R., Julius, J. & Dacks, A.M. Heterogeneous receptor expression underlies non-uniform peptidergic modulation of olfaction in Drosophila. *Nat. Comm.* **14**, 5280 (2023).
112. Schlegel, P. et al. Whole-brain annotation and multi-connectome cell typing of Drosophila. *Nature* **634**, 139–152 (2024).
113. Dorkenwald, S. et al. Neuronal wiring diagram of an adult brain. *Nature* **634**, 124–138 (2024).
114. Dacks, A. M., Riffell, J. A., Martin, J. P., Gage, S. L. & Nighorn, A. J. Olfactory modulation by dopamine in the context of aversive learning. *J. Neurophysiol.* **108**, 539–550 (2012).
115. Li, J., Ellis, K. E. & Caron, S. J. C. Photo-labeling neurons in the Drosophila brain. *STAR Protoc.* **2**, 100381 (2021).
116. Burgess, H. A. & Granato, M. Sensorimotor gating in larval zebrafish. *J. Neurosci.* **27**, 4984–4994 (2007).
117. Pfeiffer, B. D. et al. Refinement of tools for targeted gene expression in Drosophila. *Genetics* **186**, 735–755 (2010).
118. Pfeiffer, B. D., Truman, J. W. & Rubin, G. M. Using translational enhancers to increase transgene expression in Drosophila. *Proc. Natl Acad. Sci. USA* **109**, 6626–6631 (2012).
119. Dionne, H., Hibbard, K. L., Cavallaro, A., Kao, J.-C. & Rubin, G. M. Genetic Reagents for Making Split-GAL4 Lines in Drosophila. *Genetics* **209**, 31–35 (2018).
120. Tirian, L. & Dickson, B. The VT GAL4, LexA, and split-GAL4 driver line collections for targeted expression in the Drosophila nervous system. *BioRxiv*. https://doi.org/10.1101/198648 (2017).

121. Ito, K., Sass, H., Urban, J., Hofbauer, A. & Schneuwly, S. GAL4-responsive UAS-tau as a tool for studying the anatomy and development of the Drosophila central nervous system. *Cell Tissue Res.* **290**, 1 (1997).
122. Dana, H. et al. High-performance calcium sensors for imaging activity in neuronal populations and microcompartments. *Nat. Methods* **16**, 649–657 (2019).
123. Perkins, L. A. et al. The transgenic RNAi project at Harvard Medical School: resources and validation. *Genetics* **8**, 843–852 (2015).

Acknowledgements

This work was funded by NIH DC-016293 Award (AMD), NSF IOS 2114775, AFOSR DURIP FA9550-19-1-0179 and FA9550-20-1-0098 (AMD), a Grant-In-Aid of Research (G20141015669888) from Sigma Xi, The Scientific Research Society to TRS, NIH T32 GM132494 to OMC, NIH T32 GM133369 to JWH, and NIH EY036226, NIH GM144230, and NSF OIA-2242771 to EJH. We thank the Bloomington Drosophila Stock Center for their invaluable service which is supported by NIH P40 OD018537. We also thank Kristyn Lizbinski and Kevin Daly for thoughtful comments on the manuscript, Kaleb Hatch for technical assistance, and Dr. Tzumin Lee, Dr. Marco Gallio, the Janelia Research Campus Fly Core, and Dr. Hermann Dierick for providing fly stocks. We thank the Princeton FlyWire team and members of the Murthy and Seung labs, as well as members of the Allen Institute for Brain Science, for the development and maintenance of FlyWire (supported by BRAIN Initiative grants MH117815 and NS126935 to Murthy and Seung). We also acknowledge members of the Princeton FlyWire team and the FlyWire consortium for neuron proofreading and annotation.

Author contributions

Conceptualization, J.J., M.M. and A.M.D.,; Methodology, J.J., M.M., M.M.B., J.W.H., K.L.R. and A.M.D.; Formal analysis, J.J., M.M., J.W.H.; Investigation, J.J., M.M., O.M.C., M.M.B., T.R.S., J.R., J.D.R., J.W.H., F.S., E.J.F., D.E.M. and A.M.D.; Writing–Original Draft, J.J., M.M., T.R.S. and A.M.D.; Writing–Review & Editing, J.J., M.M., T.R.S., E.J.H., J.W.H., and A.M.D.; Visualization, J.J., M.M., T.R.S., J.D.R., J.W.H., F.S., E.J.F., D.E.M. and A.M.D.; Supervision, A.M.D.; Funding Acquisition, E.J.H. and A.M.D.

Competing interests

The authors declare no competing interests.

Additional information

Supplementary information The online version contains supplementary material available at https://doi.org/10.1038/s41467-025-66107-x.

Correspondence and requests for materials should be addressed to Andrew M. Dacks.

Peer review information *Nature Communications* thanks anonymous reviewer(s) for their contribution to the peer review of this work. A peer review file is available.